In Vivo Near-Infrared Fluorescence Imaging

2

Guofeng Liu, Jianhui Sheng, and Yanli Zhao

Contents

1 Definition of the Topic 67
2 Overview 68
3 Introduction 68
4 Experimental and Instrumental Methodology 70
4.1 Confocal Laser Scanning Microscopy (CLSM) 70
4.2 Two-Photon Fluorescence Microscopy 71
4.3 Fluorescence Lifetime Imaging Microscopy (FLIM) 72
5 Key Research Findings 72
5.1 Organic Fluorophores 72
5.2 Nanoparticles 82
6 Conclusions and Future Perspective 110
References 112

1 Definition of the Topic

In vivo near-infrared (NIR) fluorescence imaging used for clinical diagnostics and treatment monitoring provides a noninvasive approach for visualizing and peering deeply morphological details of tissues or living subjects with subcellular resolution.

G. Liu · J. Sheng
Division of Chemistry and Biological Chemistry, School of Physical and Mathematical Sciences, Nanyang Technological University, Singapore, Singapore

Y. Zhao (✉)
Division of Chemistry and Biological Chemistry, School of Physical and Mathematical Sciences, Nanyang Technological University, Singapore, Singapore

School of Materials Science and Engineering, Nanyang Technological University, Singapore, Singapore
e-mail: zhaoyanli@ntu.edu.sg

C. S. S. R. Kumar (ed.), *Nanotechnology Characterization Tools for Biosensing and Medical Diagnosis*, https://doi.org/10.1007/978-3-662-56333-5_2

In this chapter, we describe the applications of organic dyes, metal complexes, fluorescent biomacromolecules, and nanoparticles (such as polymers, quantum dots (QDs), carbon-based nanomaterials, upconversion nanoparticles (UCNPs), noble metal clusters, and Si-based hybrid nanoparticles) for NIR fluorescence imaging of living subjects.

2 Overview

Fluorescence is a useful noninvasive tool for visualizing the morphological details in vivo with subcellular resolution and for effective medical diagnosis and therapeutics. Except for high sensitivity and high spatial resolution, it possesses fast imaging, low-cost, and facile multiplexing properties. Thus, ideal contrast agents with bright fluorescence, desirable excitation and emission wavelength, high photostability, small size, and good biocompatibility are vital for fluorescence imaging in vivo.

However, the major obstacle of fluorescent imaging in vivo is limited by the tissue attenuation and autofluorescence. To minimize these effects, scientists have focused on NIR fluorescent probes that are excited and emitted in the spectral range of 650–950 nm, since tissues are virtually transparent and have typically no autofluorescence in this optimal NIR region. Compared with UV or visible light excitation, in vivo imaging excited from NIR light has noticeable advantages including deep penetration, weak autofluorescence, minimal photo-bleaching, and low phototoxicity. Especially, two-photon-excited fluorescence imaging on account of the anti-Stokes luminescence process provides a powerful approach to reduce autofluorescence for bioimaging. Furthermore, in vivo NIR fluorescence bioimaging is important to explore fundamental biological mechanism and pathological progression and offers key information to the disease diagnosis and therapy. An equally important issue worth to study is to invasively outline the healthy tissues from diseased ones. Thus, these methods require further optimization of design to gain effective NIR imaging agents with high brightness, excellent biocompatibility, good water solubility, and tissue-specific targeting ability.

Herein, we describe how to employ NIR fluorescent organic dyes, biomacromolecules, metal complexes, and nanoparticles (such as QDs, UCNPs, carbon-based nanomaterials, noble metal clusters, polymers, and Si-based hybrid nanoparticles) with NIR excitation or emission for fluorescence imaging in vivo in order to clearly define the physical margins of tumorous and vital tissues for disease diagnostics and therapy.

3 Introduction

Although biomedical imaging technologies have been developed for disease diagnosis and therapy, researchers still face great challenges in precisely viewing and understanding the disease processes, since these processes usually occur at the subcellular and molecular levels [1]. To date, a variety of techniques have been

used for imaging the structures and functions of bio-samples, which include ultrasound imaging, computed tomography (CT), magnetic resonance imaging (MRI), positron-emission tomography (PET), single-photon emission tomography (SPET), and optical imaging (bioluminescence and fluorescence imaging). Among these techniques, fluorescence provides a unique path to noninvasively visualize morphological details of living cells and animals with high resolution and becomes a useful tool for in vivo imaging. Unlike CT and PET imaging techniques, fluorescence imaging utilizes nonionizing and noninvasive radiation that can visualize the targeted tissue in situ with high spatiotemporal resolution in a real-time manner [2, 3].

However, there are still some limitations existing in fluorescent imaging, such as the interference from less penetration depth of light, tissue attenuation, and autofluorescence. To address these problems, various fluorescent probes with NIR excitation and emission have been continuously designed and developed. In contrast to visible light excitation for in vivo imaging, NIR light excitation possesses many merits including deep tissue penetration, weak autofluorescence, minimal photobleaching, low light scatter, and less phototoxicity, thus allowing engineered contrast agents to operate effectively by avoiding the disruptive background signal present at lower wavelengths. These properties are highly important for future clinical translation and should be maintained throughout the developmental process. These characteristics afford high signal-to-background ratio (SBR) that is recognized as the paramount parameter for successful contrast agents. High SBR paired with cost-effective lasers and detectors as well as the inherent innocuous nature of NIR light makes NIR fluorescence imaging a promising technology for further development.

Currently, many kinds of NIR fluorescent probes lie within this research focus, including small-molecule fluorophores (such as cyanines, porphyrin-based fluorophores, squaraine-based fluorophores, and metal complexes), biological species (such as fluorescent proteins and DNA aptamers), and synthetic nanoparticles (such as polymers, QDs, UCNPs, carbon-based nanomaterials, noble metal clusters, and Si-based hybrid nanoparticles).

In vivo NIR fluorescence imaging is important to explore fundamental biological mechanism and pathological progression and provides lots of important information for disease diagnosis and therapy. Specific, sensitive detection of tumors in patients is a long-standing challenge in oncology. Successful detection of small premalignant lesions and diagnosis of early-stage tumors can significantly benefit cancer treatment and improve the survival rate for patients. To improve the target-to-background ratio, fluorescent labels are typically conjugated to a tumor-targeting moiety, instead of exploiting passive dye accumulation resulting from the enhanced permeability and retention effect (EPR) of tumors. Many affinity scaffolds against cancer markers have been developed for in vivo tumor targeting, ranging from conventional antibodies and peptide-based probes to receptor-targeted natural ligands, small-molecule antagonists, and DNA or RNA aptamers. All of these representative agents must be tailored to achieve sufficient stability, specificity, and safety for human use. Before NIR imaging could be successfully employed in the clinic, contrast agents must be designed to satisfy a very particular set of parameters that are requisite to future success. The research efforts place an emphasis on improvements in terms of low

cytotoxicity, high photostability, NIR emission, two-photon excitation, and long fluorescence lifetime, which are crucial for longtime tracking of biological processes, tissue and body imaging with deep penetration and low autofluorescence, and time-resolved fluorescence imaging.

Recent advances in bioimaging provide great promises to fulfill the requirements, as targeted contrast agents have been successfully developed for visualizing both tumors and vital tissues by simultaneously utilizing spectrally different fluorophores. These tissue-specific contrast agents can be versatile warehouse to physicians for real-time intraoperative navigation and image-guided targeted therapy. NIR fluorescence light has played an important role in clinical bioimaging via providing highly specific fluorescent images of targeted tissues. Further research requires optimizing designs to gain effective NIR imaging agents with high brightness, good water solubility, excellent biocompatibility, and tissue-specific target ability.

Although there are many reviews highlighting organic fluorophores and nanoparticles for fluorescence imaging [1–56], there is still no review to systematically summarize various organic fluorophores and nanoparticles with NIR fluorescence for in vivo bioimaging. Herein, we discuss recent significant research progress about NIR fluorescent probes, including small-molecule fluorophores, biological species, and synthetic nanoparticles, for in vivo NIR fluorescence bioimaging.

4 Experimental and Instrumental Methodology

4.1 Confocal Laser Scanning Microscopy (CLSM)

CLSM is a noninvasive optical imaging technique with high contrast and resolution of images through the addition of a spatial pinhole placed at the confocal plane of the lens to eliminate out-of-focus light. This technique has been widely employed in bioimaging applications. It enables the reconstruction of three-dimensional structures from sets of images obtained at different depths within a thick object, although the penetration depth of CLSM is restricted and only acquires images one depth level at a time. Currently, CLSM has been used for fixed or slowly evolving cellular structures due to its noninvasiveness, high resolution, and real-time optical sectioning capabilities. For instance, upconversion-enabled optical microscope usually comprises an inverted microscope, an NIR (980, 915, or 808 nm) continuous wave (CW) diode laser, a charge-coupled device (CCD) camera, and optical components like dichroic beam splitter and excitation and emission filters. A CLSM setup for upconversion-based imaging based on an inverted microscope and a confocal scanning unit is depicted in Fig. 2.1 [57]. The CW laser emitting at 980 nm is conducted by galvanometer mirrors and then focused by objective lens into the specimen. Light emitted from the location of the scanning spot is deflected by the galvanometer mirrors, separated from the excitation by a reverse excitation dichroic mirror, passed through a confocal pinhole and a filter, and finally captured by a detector consisting of photomultiplier tubes. Multiplexed imaging can be simultaneously

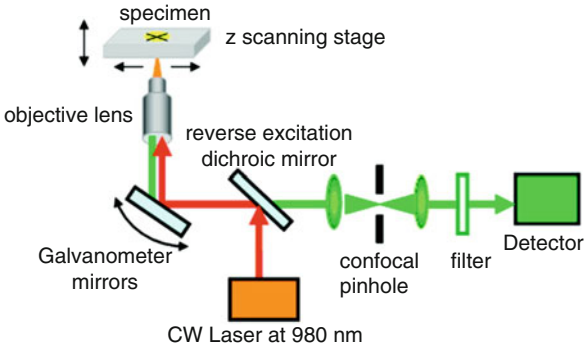

Fig. 2.1 Schematic illustration of a laser scanning upconversion luminescence microscopy (LSUCLM) system setup. The excitation laser beam pathway is depicted in red, and the emission path is displayed in green [57] (Reprinted with permission from Ref. [57], Copyright 2009 the American Chemical Society)

obtained by detecting individual emission wavelength channels. In addition, live cell incubator systems can enable long-term and real-time tracking of cells.

For upconversion luminescence (UCL) in vivo imaging, UCNP dissolved in physiological saline is injected into specially targeted site of mice. After being anesthetized, mice are imaged by utilizing an NIR optical fiber-coupled laser as the excitation source under a safe power (usually no more than 0.2 W/cm^2). A short-pass emission filter is used to prevent the interference of excitation light to the CCD camera. In vivo spectral imaging is carried out with a rate of 10 nm per step and with an enough exposure time due to rather low quantum yield of UCNPs.

4.2 Two-Photon Fluorescence Microscopy

Two-photon fluorescence (TPF) microscopy (Fig. 2.2) is a noninvasive imaging technology for cell and tissue imaging, which shows enhanced penetration depth, increased spatiotemporal resolution, diminished tissue autofluorescence interference, and reduced photodamage as compared to one-photon imaging. Unlike in the case of traditional fluorescence microscopy, the shorter wavelength of emitted light in TPF microscopy is excited by the longer wavelengths of two exciting photons. Generally, the excitation lights employed for TPF technology are in the NIR region. Using NIR light can highly minimize the scattering from the tissues, leading to an increased penetration depth for bioimaging. Meanwhile, the background signal is also greatly suppressed because of the two-photon absorption. Thus, two-photon excitation can be a superior alternative to confocal microscopy because of its deeper tissue penetration, efficient light detection, and reduced phototoxicity.

For two-photon in vivo imaging experiments, mice are first anesthetized and subsequently injected with the solution of NIR fluorescent probes at the targeted area. The images are obtained by utilizing a two-photon microscope with a tunable 680–1080 nm laser. When using zebra fish as animal models, zebra fish are first incubated with NIR fluorescent probes [59]. After washing with PBS (pH 7.4) to remove the remaining probe, TPF fluorescence images are observed under multi-photon laser scanning confocal microscope using a mode-locked titanium-sapphire laser source set at a targeted wavelength with suitable laser power.

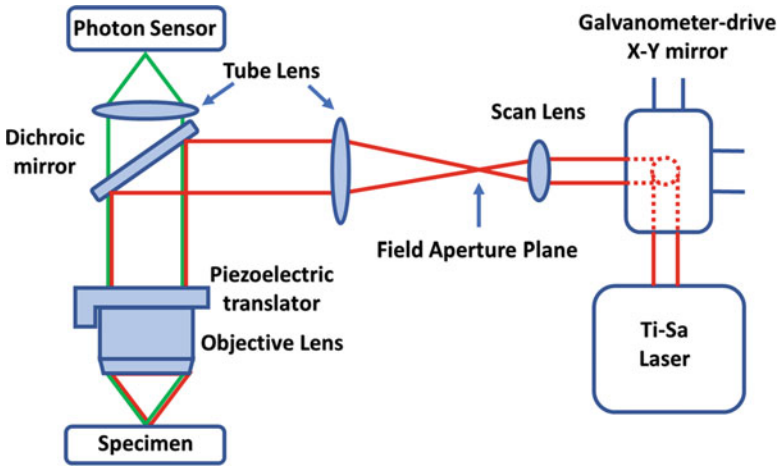

Fig. 2.2 Schematic illustration of two-photon microscope. The excitation laser beam path is shown in red, and the emission pathway is displayed in green [58] (Reproduced with permission from Annual Reviews, Copyright 2000)

4.3 Fluorescence Lifetime Imaging Microscopy (FLIM)

Apart from imaging techniques based on luminescence intensity, FLIM can offer images by measuring the emission lifetime of a signal. The main merit of FLIM is that it can provide quantitative information and monitor cellular dynamic activities with high spatial resolution [14]. Generally, a pulsed light source is necessary, and time-correlated single-photon counting (TCSPC) is adopted in common FLIM. To carry out FLIM, an external frequency-doubled picosecond Nd:YAG laser, operating at 532 nm with a pulse width of 7 ps and a frequency of 50 MHz, is coupled through a single-mode optical fiber into the Leica microscope featuring a FLIM system (Fig. 2.3). Fluorescence is measured by using a 63× oil-immersion objective and detected with an APD at a wavelength of 650–850 nm through a band-pass filter. A time-correlated single-photon counting system is applied to detect the fluorescence lifetime, where time-gated images are acquired with the SymPhoTime software.

5 Key Research Findings

5.1 Organic Fluorophores

Organic fluorophores including NIR dyes, fluorescent proteins, DNA aptamer, and metal complexes are widely used NIR-emitting molecules for bioimaging due to their versatile structures and facile synthesis. In this section, we will discuss the utilizations of these organic fluorophores for NIR imaging.

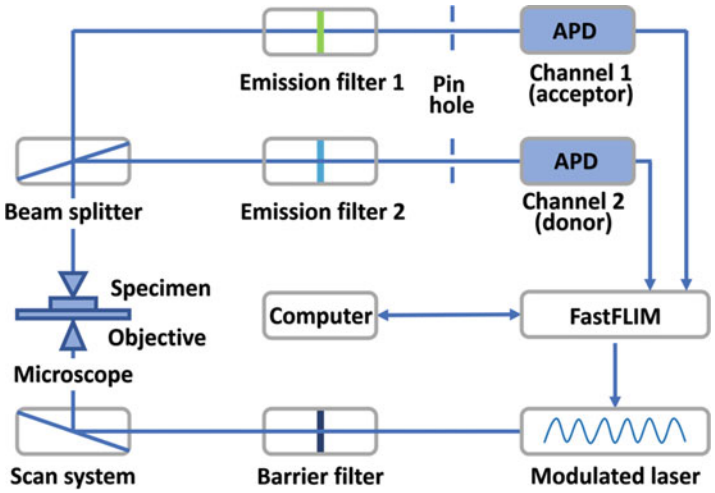

Fig. 2.3 Schematic illustration of the experimental FLIM setup

5.1.1 NIR Dyes

Inspired by fascinating colors of dyes widely used in staining, chemists and materials scientists have greatly widened the applications of fluorescent dyes for in vivo imaging [8–10, 18, 35, 39, 40, 49, 60–64]. Particularly, great zeal has been focused on NIR dyes whose absorption and emission lie in the region of 750–900 nm, since tissues are virtually transparent and have no autofluorescence in this NIR window. Up to now, a large number of NIR fluorescent dyes have been designed and developed for in vivo imaging, such as cyanines [65], porphyrin-based fluorophores [66], xanthene dyes [67, 68], squaraine rotaxanes [26], and phenothiazine-based fluorophores [69]. All of these representative agents are tailored to achieve sufficient stability, specificity, and safety for practical use [39].

Cyanine dyes, as well-known NIR fluorochromes, are usually featured by polymethine chain bridged with two aromatic heterocycles containing nitrogen [70–72]. The absorption and emission of cyanine can be adjusted to NIR region by altering the length of polymethine bridge with the addition of vinylene group to achieve about a 100 nm bathochromic shift. Generally, cyanine dyes are weakly luminescent, since the polymethine bridge in the excited state is flexible and easy to the isomerization [73]. To enhance the quantum yield of cyanine, an effective approach is to stiffen the backbone by introducing chlorocyclohexenyl moiety on the polymethine chain [71]. Traditional cyanine dyes, in essence, are easy to aggregate in aqueous solution. Fortunately, the phenomenon of self-aggregation can be largely alleviated by the introduction of two sulfonate groups to the nitrogen-containing heterocycles. Poor photostability is a major limitation for cyanine dyes, since the fluorophore molecules are quite sensitive to the dissolved oxygen. A promising approach to enhance the photostability is incorporating cyanines into the silica nanoparticles where the nanoparticle shell can effectively protect

the fluorophore molecules. Due to the excellent biocompatibility, a variety of cyanine-based dyes with NIR florescence were effectively used for medical diagnostic imaging in vivo [74–77].

A typical strategy for constructing targeted fluorescent imaging agents requires covalently conjugating the separate target and fluorophore domains. On the other hand, it is possible to develop a single NIR fluorophore-based perform with both targeting and imaging by their inherent chemical structures [76]. For instance, NIR contrast agents were developed to target cartilage with high specificity and performed well for biomedical imaging of bone in vivo [78, 79]. By conjugating with biofunctional groups, zwitterionic NIR fluorophore based on cyanine outperforms commercially available NIR fluorophores IRDye800-CW and Cy5.5 in vivo for image-guided surgery [80]. Recently, NIR fluorescence probes based on cyanine were used for noninvasive in vivo imaging of endogenous H_2S without interfering with biological autofluorescence and for detecting tumors in mice [77]. Covalently conjugating cyanine dye with human serum albumin (HSA) was also used to conduct multimodality (NIR fluorescence/photoacoustic/thermal) imaging and eliminate tumor by intravenously injecting the nanosystem into tumor-bearing mouse model [75]. In addition, it is useful to specifically image different tissues by NIR fluorophores based on their inherent chemical structures. For example, a halogenated fluorophore based on cyanine dyes with NIR emission has been synthesized to successfully identify and preserve parathyroid and thyroid glands in vivo. By means of dual-channel NIR imaging approach, parathyroid and thyroid glands can be unambiguously observed and distinguished in the coexisting blood and surrounding soft tissues [81]. Unlike cationic cyanine, pyrrolopyrrole cyanine (PPCy) is a nonionic cyanine-type dye with NIR absorption and emission, which is favorable for bioimaging after the biofunctionalization [82].

Squaraine dyes are featured with resonance-stabilized zwitterionic structures and consist of a central oxocyclobutenolate-based core linked with two aromatic or heterocyclic moieties on both sides [83–87]. Squaraines usually show sharp and intense absorption and emission bands, which are ascribed to the unique donor-acceptor-donor (D-A-D) electron-transfer structure. However, most of them are water-insoluble and emit below 600 nm with low extinction coefficients, making them unsuitable for deep tissue imaging. Furthermore, the strong tends to aggregate, and the susceptibility of the central cyclobutene ring to undergo chemical attack greatly impede their usage for in vivo imaging [83, 85–87]. These drawbacks can be favorably overcome by the physical encapsulation of squaraines in tetralactam macrocycles. Based on this strategy, various NIR-emissive squaraine dyes were synthesized for in vivo imaging [88]. For example, unsymmetrical NIR squaraines (USq) was successfully developed as an exogenously produced fluorescent probe for fluorescence and photoacoustic imaging of thiol variations in vivo [83]. USq absorbs a wavelength of 680 nm and emits a strong NIR emission at 700 nm, which is suitable for deep tissue fluorescence imaging. Dependent on the presence of different thiols, the fluorescence and photoacoustic signals can selectively disappear. Upon food uptake, bright imaging of aminothiols in blood can be confirmed by in vivo imaging (Fig. 2.4).

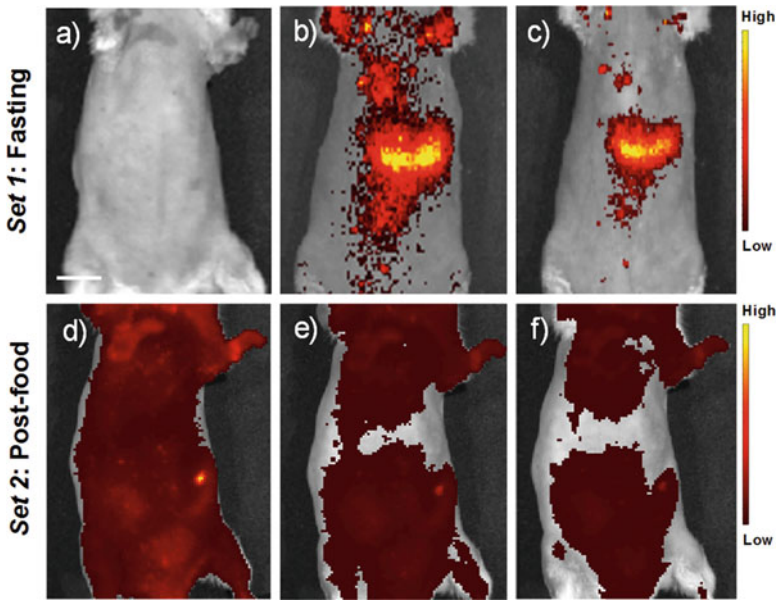

Fig. 2.4 (**a**–**f**) In vivo fluorescence images acquired from postinjection of USq in fasting (set 1) and post-food (set 2) mice [83] (Reprinted with permission from Ref. [83], Copyright 2016 the Royal Society of Chemistry)

Boron dipyrromethenes (BODIPYs) can be regarded as rigid cross-conjugated cyanine dyes with small Stokes shifts but high molar extinction coefficients [89–94]. Moreover, spectroscopic properties of BODIPYs show sharp spectra, shiny fluorescence, high quantum yields, and less influence by solvent polarity and pH [18]. Small chemical modifications on BODIPY structures could induce large emission shifts and improve water solubility as well as the extinction coefficient [72, 73, 95, 96]. The combined features of BODIPYs make them a useful platform to develop NIR-emitting contrast agents for in vivo imaging [63]. Generally, the absorption and emission of pristine BODIPY core exhibit at ~500 nm, but it can be shifted in the NIR regions via various strategies of extending the conjugation length or reducing the resonance energy [89, 90, 92]. Compared with phenyl-substituted counterpart, the absorption and emission of aza-BODIPY attached with thiophene at 1-, 3-, 5-, and 7-positions redshift to 733 and 757 nm, respectively [91]. For example, an NIR-emitting probe based on BODIPY showed non-fluorescence with Cu(II). When injected with Na_2S in mouse, it performed a remarkable fluorescence "switch on" response at 790 nm [97]. More and more NIR fluorophores based on BODIPY were successfully constructed for imaging in vivo with high selection and sensitivity [96–98]. For instance, aniline-substituted aza-BODIPY with pH-response was employed to selectively image tumor. Meanwhile, photodynamic therapy (PDT) and therapeutic self-monitoring were also achieved via encapsulating it in cRGD-functionalized micelle (Fig. 2.5) [98].

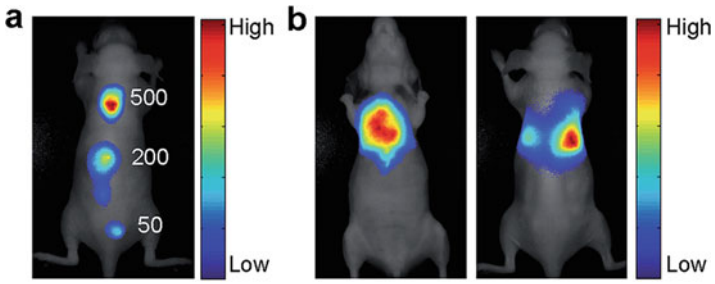

Fig. 2.5 (**a**) In vivo NIR fluorescence imaging sensitivity and (**b**) depth of U87MG cells labeled with cRGD-Net_2Br_2BDP NP [98] (Reprinted with permission from Ref. [98], Copyright 2015 the Royal Society of Chemistry)

Xanthene dyes, as a type of classical fluorophores, possess good photostability and moderate hydrophilicity [15]. After rational chemical modifications, they show excellent NIR emission and are favorable for biological imaging applications in living animals [99–102]. For example, several rhodamine-based NIR dyes were developed for imaging endogenously generated HClO in the living animals [101]. Moreover, NIR fluorescent Si-rhodamine dyes were developed to be powerful labeling tools for multicolor bioimaging [102].

Porphyrins are conjugated tetrapyrrolic macrocycles and considered as "pigments of life," thanks to their extensive presence in biological systems [103–105]. Due to outstanding and versatile features, porphyrins can be easily functionalized and undergo various supramolecular interactions [104]. The remarkable and strongly tunable luminous features of porphyrinoids enable them with a great potential for bioimaging with strong NIR emission [103]. Up to now, an effective approach to gain bright NIR fluorescence is to extend the conjugation of ring. This strategy has been demonstrated by the expansion of ring conjugation in Pt(II)-porphyrins through exploring the substituent effect in *meso* positions [105]. Porphysomes were developed from self-assembled porphyrin bilayers, which possess large extinction coefficients, structure-dependent fluorescence, and unique photothermal and photoacoustic features. The optical features and relatively good biocompatibility of porphysomes prove the multimodal potential of organic fluorophores for bioimaging and therapy [106]. For example, a cleavable folate-photosensitizer conjugate was successfully used for both NIR fluorescence imaging and PDT of cancer cells with high specificity (Fig. 2.6) [107].

Phthalocyanines, termed tetrabenzotetraazaporphyrins, are analogs of tetrabenzoporphyrins containing N atoms in the *meso* position of the ring in place of C atom. They are featured by two sets of absorption bands in the UV-Vis region. One called B band is located at around 350 nm, and the other one termed Q band is placed in the region of 600–700 nm. It should be noted that protonation could cause remarkable redshift of the Q band and accordingly the emission peak is present at

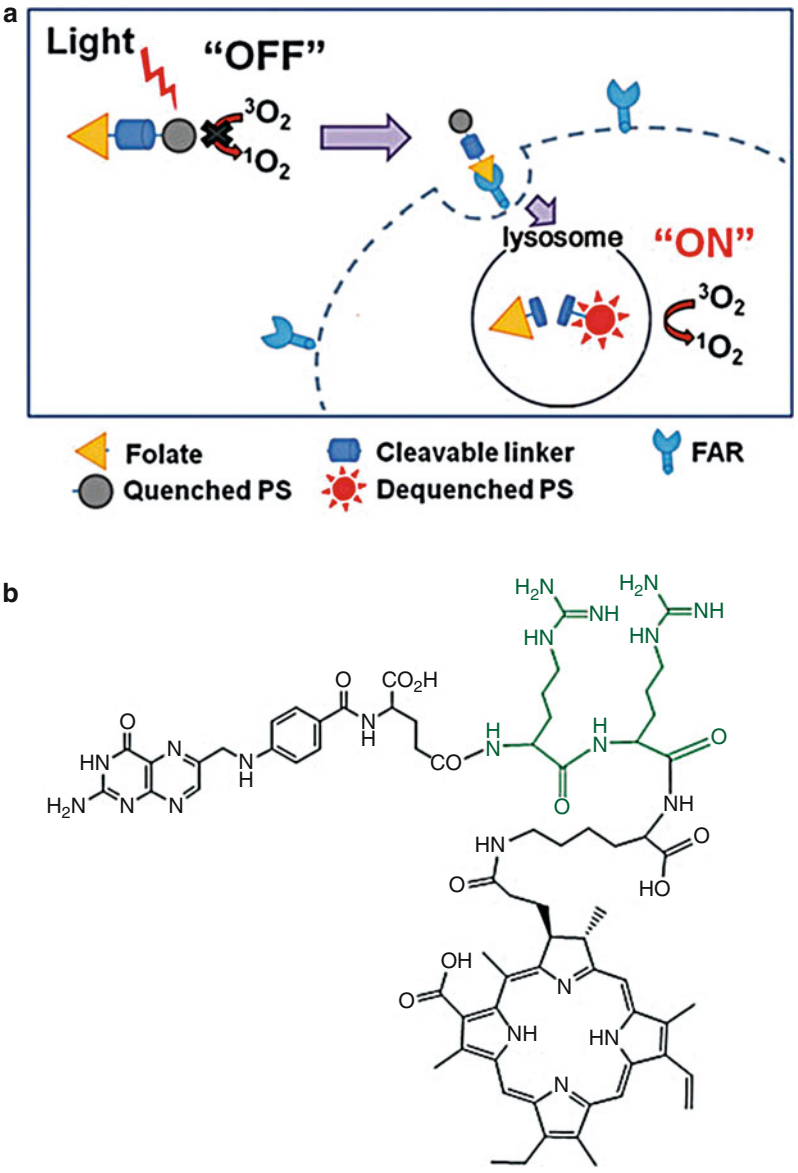

Fig. 2.6 (**a**) Schematic illustration of cleavable folate-photosensitizer conjugate for NIR fluorescence imaging and photodynamic therapy. (**b**) Chemical structure of the conjugate [107] (Reprinted with permission from Ref. [107], Copyright 2014 the Royal Society of Chemistry)

longer wavelength. Moreover, it can also achieve redshift of the fluorescence and absorption by expanding the π-conjugation structure of the macrocycle [64]. Phthalocyanines can host many metal ions in the core and undergo wide chemical modifications.

Except for the abovementioned NIR fluorescent dyes, other NIR dyes or two-photon excited fluorophores were also developed for in vivo imaging [107–111]. For example, red emitting dicyanomethylenebenzopyran probe (DCMC-N_3) was successfully used to detect the presence of HS in vivo by employing two-photon microscopy [31, 112]. NIR-II molecular fluorophores based on shielding unit-donor-acceptor-donor-shielding unit (S-D-A-D-S) structure developed very recently may offer rich opportunities to improve the performance for NIR-II bioimaging [109].

5.1.2 Metal Complexes

Transition metal complexes are a versatile type of emitters that provide a series of inherent merits over traditional fluorescent materials [62]. Firstly, they show large Stokes shifts due to the S_1-T_1 intersystem crossing, which can effectively discriminate the excitation and emission light, and prevent fluorescence quenching caused by self-absorption. Secondly, the emissive excited state displays long lifetime within the range of μs to ms. Thus, metal complexes can be used for time resolution imaging. Furthermore, metal complexes such as d^6, d^8, and d^{10} metal ions – Re(I), Os(II), Ru(II), Ir(III), Pt(II), Au(III), Au(I), and Cu(I) – possess emission in the NIR region. Metal complexes exhibit high luminescence efficiency through a rational modification of ligand frameworks including the inclusion of donor-acceptor push-pull systems, the change of the π-conjugation length, or the addition of heterocycles. Thus, metal complexes present many advantages including easily tunable chemical and photophysical properties, high emission quantum yields, long phosphorescence lifetime, large Stokes shifts, and emissive properties that are highly sensitive to subtle changes in the local environment, which collectively enable metal complexes with a great potential in bioimaging [113].

Some metal complexes show two-photon absorption. Due to the excitation of NIR light in two-photon absorption metal complexes, they possess features of deep tissue penetration, weak autofluorescence, low photo-bleaching, and low phototoxicity for bioimaging [114]. For instance, by illumination with 840 nm laser, two-photon active Zn(salen) complex was employed for imaging of living cells and organism with high signal-to-noise contrast and good membrane permeability [115, 116].

5.1.3 Fluorescent Proteins

Fluorescent proteins are widely used as contrast agents for bioimaging with high spatiotemporal resolution [48, 55, 117–119]. A prerequisite for in vivo fluorescence imaging is the safety of contrast agents. As a fluorescent probe from biological system, NIR fluorescent proteins are safe enough and would be useful to increase the sensitivity of in vivo imaging [55, 120]. For instance, fluorescent proteins were used for whole-body and deep tissue imaging to explore the metastasis, cell migration, tumor distribution, and embryogenesis.

To obtain the fluorescent proteins with NIR excitation and emission, several feasible approaches have been developed. A useful strategy is the exploration of phytochromes for NIR fluorescence imaging. Phytochromes root in plant and

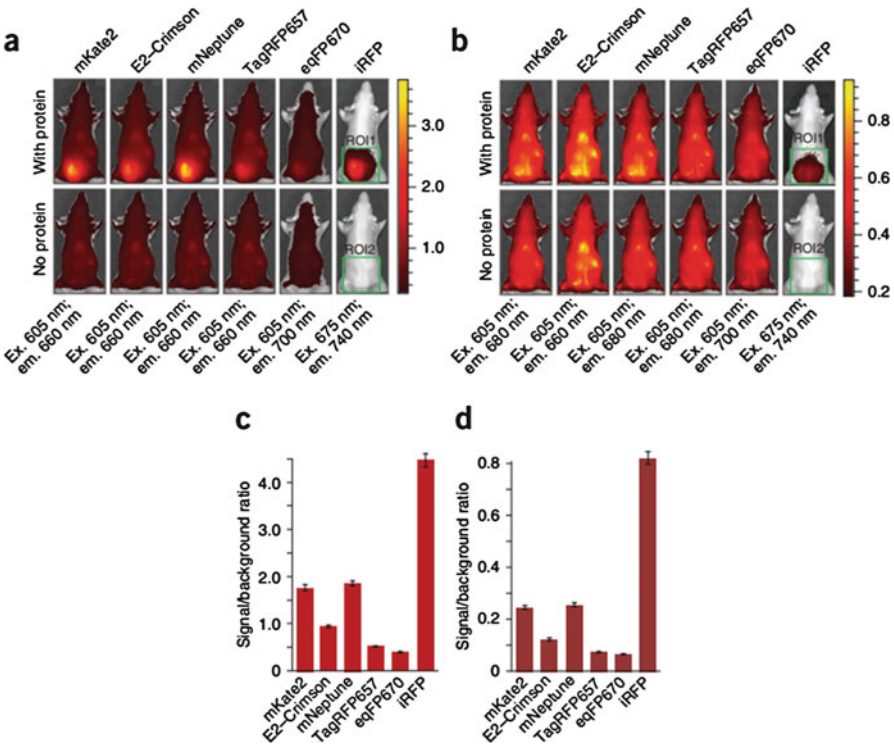

Fig. 2.7 (**a**–**d**) Comparison of near-infrared fluorescent protein (NIRFP) with far-red GFP-like proteins in mouse phantom [122] (Reprinted with permission from Ref. [122], Copyright 2011 Nature Publishing Group)

bacterial photopigments, which can absorb NIR light and emit weak fluorescence. Through chemical modifications, engineered NIR fluorescent proteins from phytochromes show excellent NIR absorption and good aqueous quantum yield [117]. For example, NIR fluorescent proteins selected by using bacterial expression method showed low toxicity in bacterial expression experiments. After distributed in mice, they presented relatively high brightness and no toxicity [121]. In contrast to far-red green fluorescent protein (GFP)-like proteins, NIR fluorescent proteins display a considerably higher SBR in mice because of their infrared-shifted spectra. NIR fluorescent probes could facilitate the imaging of biological processes in living tissues with low autofluorescence and light scattering. For example, NIR fluorescent proteins with bright luminescence were used to label live mammalian cells and show low scattering and absorption in most tissues (Fig. 2.7) [122]. The bright phytochrome-based proteins are stable and low cytotoxic and exhibit bright fluorescence in both tissues and whole animals with high SBR.

Fluorescent proteins with bright NIR emitting are undoubtedly suitable for whole-body imaging in vivo. However, it is not easy to develop fluorescent proteins with NIR emission. Proteins labeled with NIR fluorescent dyes would be an

alternative approach for targeted tumor imaging with NIR light. Epidermal growth factor receptor (EGFR) protein, a vital transmembrane protein in the family of tyrosine kinase receptors, plays an important role in physiological and pathological processes. Since aberrant overexpression of EGFR is related to many kinds of cancers, it was used for noninvasive imaging of tumor in vivo. For example, Eaff800, an EGFR-specific Affibody molecule labeled with NIR fluorescent dye IRDye800CW maleimide, was successfully used to identify A431 xenograft tumor in mice. Interestingly, combined with a human EGFR type 2 (HER_2), Eaff800 could clearly distinguish the overexpression of EGFR and HER_2 in tumors by showing different organ distribution pattern and clearance rate [123].

Fluorogen-activating proteins (FAPs) are single-chain variable fragment-based fluoromodules that bind to non-fluorescent dyes (fluorogens), yielding thousandfold fluorescence enhancements. It can specifically bind targeting moieties and activate non-fluorescent dyes to visualize tumor with low nonspecific tissue staining, high contrast, fast clearance, and good tissue penetration. Affibodies, small peptides of 58 amino acids with high affinity and specificity to target proteins, are used to conjugate organic fluorophores and fluorescent proteins (affiFAP) for in vivo tumor imaging. Alternatively, FAPs binding to triphenyl methane analogs of malachite green (MG) dyes with NIR fluorescence emission may also be helpful, where probes can be targeted to a tumor site and fluorogens added serve for fluorescence visualization. For example, an FAP/MG complex was successfully employed to prepare responsive fluorescence probes for in vivo tumor imaging. Compared with conventional fluorophore-conjugated Affibodies, preincubated affiFAP/fluorogen complex could label EGFR-enriched tumors with similar perivascular tumor distribution but with higher target specificity. Due to specific fluorescence activation upon the FAP binding, no nonspecific background fluorescence was observed. The rapid FAP/fluorogen association and probe clearance allowed either sequential administration of probe and dye or local dye application with high tumor-to-background ratio (TBR). The fluorogen activation, coupled with rapid clearance of unbound small-molecule fluorogen when employing a pre-targeting approach, should significantly reduce background fluorescence from probes. Stepwise labeling can potentially provide more temporal and spatial control during the labeling procedure [124]. This pre-targeted activation approach may substantially improve the TBR and highly enhance the sensitivity for early or residual tumor diagnosis and surgery.

Directly conjugated IR dyes possess useful properties for in vivo imaging, but the conjugation often substantially alters the circulation dynamics of targeting moieties. A new tumor-targeting probe, affiFAP, was developed, which consists of an FAP and a protein that specifically binds EGFR (Affibody) [125]. This compact molecular recognition reagent can reversibly bind and activate fluorescence of otherwise non-fluorescent dyes and allows tumor visualization with low nonspecific tissue staining. Molecular pre-targeting of affiFAP with fluorogenic dye was employed to achieve high contrast, fast clearance, and good tissue penetration. Due to the instability of proteins, fluorescent proteins are still not employed for in vivo imaging in the purified form. By coating an NIR fluorescent protein with a silica nanoshell, the obtained system showed high quantum yield and photostability due to the

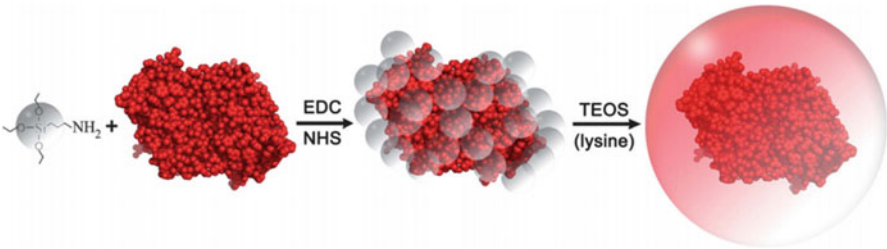

Fig. 2.8 Schematic layout of procedures for individually coating NIR fluorescent protein with a silica nanoshell [126]. *EDC* 1-ethyl-3-(3-dimethylaminopropyl)carbodiimide hydrochloride, *NHS* *N*-hydroxysuccinimide, *TEOS* tetraethyl orthosilicate (Reprinted with permission from Ref. [126], Copyright 2013 the Royal Society of Chemistry)

protection of silica shell and can be successfully used as safe and robust NIR fluorescence probe for whole-body imaging of mouse via the injection from the tail vein (Fig. 2.8) [126].

5.1.4 Aptamers

Aptamers are single-stranded DNA or RNA and can specifically recognize their targets. For instance, aptamers could be integrated into the DNA nanostructures either via base pair hybridization or as a component in the assembly procedure. DNA nanostructures have good biocompatibility, high tissue penetration, and sufficient stability in biofluids, enabling them for in vivo imaging. Due to inherent binding abilities of aptamers and superior properties of DNA nanostructures, increasing attention has been focused on the establishment of aptamer-integrated DNA nanostructures for bioimaging [19, 33, 127]. In addition, aptamers with many desirable features including small size, simple synthesis, facile chemistry, and lack of immunogenicity can specifically bind to a variety of target molecules. Aptamers, engineered with substantially enhanced biochemical functions and unique specificity, are powerful in bioimaging applications [128].

Although aptamers have emerged as promising fluorescence probes for cancer imaging, limitations including limited contrast and high background still hamper their applications in bioimaging. Aptamers, conjugated with dyes or nanoparticles as activatable probes, can change their optical properties upon biological interactions for the fluorescence imaging [127]. Thus, an activatable aptamer probe (AAP) was developed to specifically bind the membrane proteins of cancer cells, exhibiting contrast-enhanced tumor visualization in vivo (Fig. 2.9). The fluorescence of AAP can be activated by undergoing a conformational change upon targeting to cancer cells. After imaging a type of cancer cells in vivo, AAP can be specifically activated by targeted tumor cells with a considerable fluorescence enhancement. In contrast to other aptamer probes, AAP performs significantly enhanced image contrast, minimal background signals, and shorten diagnosis time [129].

Aptamers have been demonstrated for target imaging of cancer cells in vivo. However, due to limited affinity and the nuclease degradation of aptamers, typical

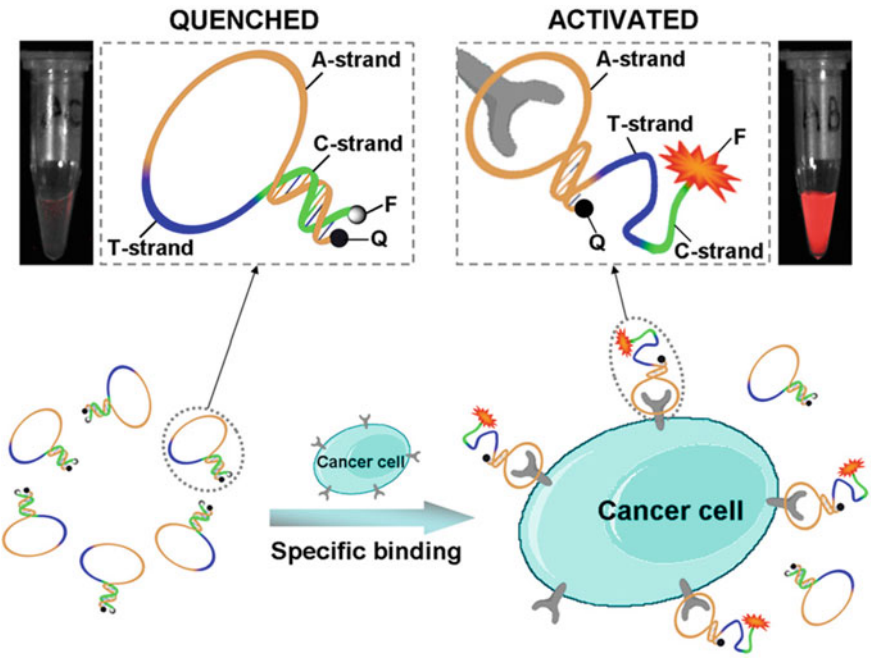

Fig. 2.9 Schematic representation of in vivo cancer imaging by using AAP on account of cell membrane protein-triggered conformation alteration [129] (Reprinted with permission from Ref. [129], Copyright 2011 National Academy of Sciences)

aptamers have not yet been used in practical in vivo imaging. Polyethyleneimine (PEI) can substantially lower the degradation rate of aptamers and improve their pharmacokinetics. Thus, PEI/aptamer molecular complexes were successfully used for tumor imaging in vivo by utilizing deoxyribonuclease (DNase)-activatable fluorescence probes (DFProbes) to detect the DNA degradation. Compared with free aptamer, the complexes exhibited excellent passive tumor targeting and prolonged circulation time in tumor-bearing mice [130].

Hybridization chain reaction (HCR), featured as multiplexed, enzyme-free, and isothermal molecular signal amplification, enables simultaneous imaging of multiple target mRNAs [131]. For instance, a multiplexed fluorescence in situ hybridization method on account of orthogonal amplification with HCR was developed to simultaneously map five target mRNAs in fixed zebra fish embryos with deep penetration, high SBR, and sharp signal localization (Fig. 2.10) [132].

5.2 Nanoparticles

Previous sections are concentrated on the advances of organic NIR fluorophores. On the other hand, there are significant advantages to locate the contrast agents inside a

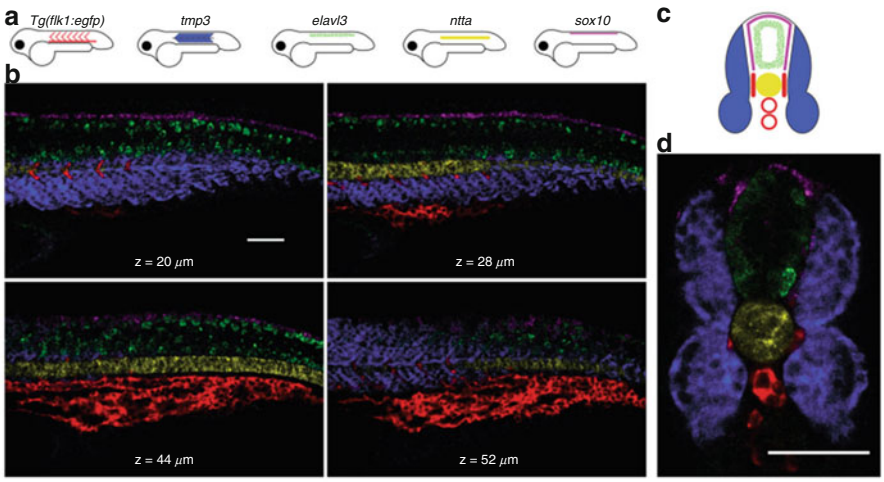

Fig. 2.10 (**a**–**d**) Multiplexed mapping in fixed whole mount and sectioned zebra fish embryos [132] (Reprinted with permission from Ref. [132], Copyright 2010 Nature Publishing Group)

nanoparticle for diagnosis and therapy. Nanoparticles with large sizes and well steric protection can effectively extend the circulation times. Generally, the preparation of nanoparticles for bioimaging contains several steps, including the synthesis, coating, surface modification, and bioconjugation. Nanoparticles with desired ligands onto their surface can be easily engineered by physical adsorption or chemisorption. Nanoparticles engineered by chemisorption not only exhibit high colloidal stability, good biocompatibility, and sufficient water solubility but also can covalently link functional groups for further bioconjugation.

The judicious design of nanoparticles with multiple functionalities has fueled significant progress in bioimaging. Fluorescent probes based on nanoparticles have blossomed in recent years thanks to their superior properties, making them hopeful alternatives to organic dyes and fluorescent proteins for cancer imaging and therapy. For instance, inorganic semiconductor QDs show much better fluorescent performance for bioimaging than traditional organic fluorophores due to their tunable emission, enhanced photostability, and high quantum yields. Thus, the rational choice of suitable nanoparticle compositions and the implement of surface functionalization would facilitate the design of fluorescent nanoparticle probes that emit enhanced fluorescence and display increased selectivity.

5.2.1 Polymer Nanoparticles

To date, polymer nanoparticles have been widely developed and used for fluorescent imaging [133–136]. In general, polymer-based nanoparticles with various morphologies can be prepared by physical encapsulation or chemical conjugation of contrast agents (such as inorganic nanoparticles or fluorescent dyes). In these nanosystems, polymers play a vital role in enhancing the aqueous stability of contrast agents,

efficiently transporting contrast agents to pathological areas, and improving the imaging [137].

Conjugated polymers (CPs), featured by a backbone with a delocalized electronic structure, were demonstrated to bind analyte receptors with obvious responses [138, 139]. To enhance the water dispersibility of neutral CPs, a variety of physical processes including nano-precipitation [140], mini-emulsion polymerization [141], and solvent extraction single emulsion [142] can be used. Usually, bare CP nanoparticles possess high photostability, good biocompatibility, and efficient permeability to cellular cytoplasm. CPs with NIR emission can be easily obtained by doping hydrophobic dyes into CP nanoparticles. Since the polymeric backbone of CPs is connected by conjugated electrons, any small perturbation of the conjugated system would result in large signal change and subsequently affect the entire assembly. Moreover, CPs with hyperbranched structures and biocompatible side chains could covalently couple many biological probes or drug molecules and efficiently transport them into live cells, which allow the diagnosis and therapy simultaneously possible. Thus, their structures and function can be tuned easily for target applications through the judicious choice of the composition and surface modification. To enhance the brightness and cell uptake efficiency, CP-based nanoparticles (CPNs) with tunable size and optics, excellent biocompatibility, and low toxicity were designed and synthesized for bioimaging [141–146].

Generally, the quantum yields of CPs would drop greatly by the nanoparticle formation. Exceptionally, cyano-substituted derivatives of poly(p-phenylene vinylene) in the aggregated film state showed efficient interchain excitonic photoluminescence in the NIR region with reasonably high quantum yields, which enabled researchers to develop NIR fluorescent probes based on CPs [147]. For instance, nanoparticle probes based on cyanovinylene backbone CPs with bright NIR fluorescence were successfully used for real-time sentinel lymph node mapping (SLNs) in mice and displayed high chromophore density and strong fluorescence, which can precisely and noninvasively identify superficial SLNs and fluorescently visualize deep SLNs (Fig. 2.11) [141].

Furthermore, polymer dots (P-dots) are an emerging class of fluorescent probes due to their large absorption coefficients, excellent brightness, high photostability, and nontoxicity [148–155]. Although the research of P-dots for bioimaging is still at an early stage, various strategies have been developed to enlarge the versatility and biofunctions of P-dots for in vivo imaging, such as tuning the emission wavelength, developing new preparation approaches, modifying the nanoparticle surface, and doping functional molecules. Recently, an emerging strategy was developed to effectively construct P-dot bioconjugates, demonstrating their features of specific cellular targeting and bio-orthogonal labeling. For example, a highly fluorescent P-dots based on CPs with benign toxicity and bright NIR emission were covalently attached with cancer-specific peptide ligands and successfully applied for target imaging of malignant brain tumors in mice (Fig. 2.12) [152].

In contrast to CPs, conjugated polyelectrolytes (CPEs) are water-soluble polymers, featuring as π-conjugated backbones and ionic side chains [12]. CPEs possess tunable size, high photostability, and good biocompatibility and can react with a

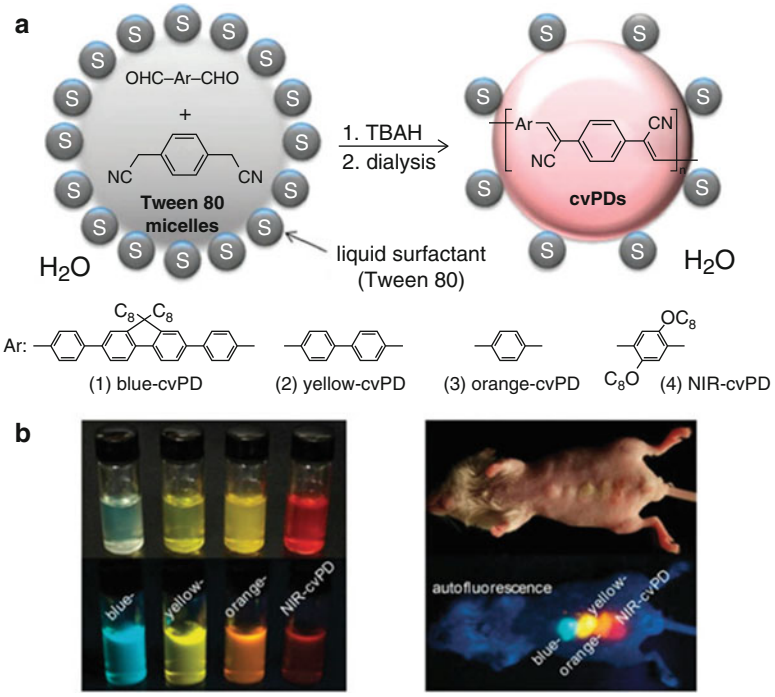

Fig. 2.11 (**a**) Schematic layout illustrating colloidal synthesis of cyanovinylene-backboned polymer dots (cvPDs). (**b**) True-color images of cvPDs (left) and a cvPD-injected live mouse (right) under room light (top) and UV excitation at 365 nm for fluorescence (bottom) [141]. TBAH, tetrabutylammonium hydroxide (Reprinted with permission from Ref. [141], Copyright 2010 the Royal Society of Chemistry)

variety of biofunctional groups and desired biorecognition elements. Similar with CPs, their absorption and emission properties can be finely tuned by backbone modifications. For example, grafted CPEs complexed with cisplatin were successfully demonstrated not only as effective contrast agents for NIR imaging in vivo but also to monitor the drug distribution in vivo by intravenous injection [156].

In addition, micellar nanocarriers containing amphiphilic block copolymers can also be developed for bioimaging, because of the drug and NIR fluorophore encapsulation capability of the hydrophobic micelle core and the biocompatibility and targeting resulted from the hydrophilic corona [157]. For example, in vivo tumor diagnosis and therapy were simultaneously achieved by using micellar nanocarriers based on the combination of pH-responsive micelle and a photosensitizer. In the system, pH-responsive micelles can efficiently deliver the encapsulated protoporphyrin IX to tumors, displaying clear imaging of tumors in vivo [158].

5.2.2 Quantum Dots

Semiconductor QDs are colloidal nanocrystals with sizes between about 1 and 10 nm close to the exciton Bohr radius. In general, each nanocrystal is composed of

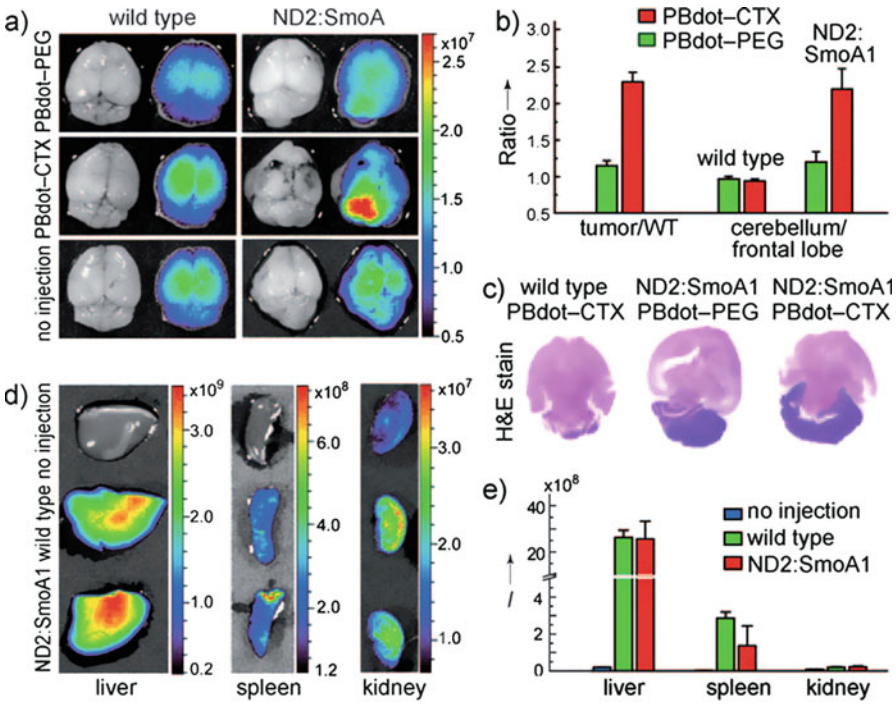

Fig. 2.12 (**a**) Fluorescence imaging of healthy brains (left) and medulloblastoma tumor ND2:SmoA1 (right) by PBdot. (**b**) Quantified fluorescence signals in ND2:SmoA1. (**c**) Histological examination of the mouse brains in (**a**). (**d**) Biophotonic images of resected livers, spleens, and kidneys from wild-type and ND2:SmoA1 mice. (**e**) Biodistribution of the PBdot probes in the resected organs [152] (Reprinted with permission from Ref. [152], Copyright 2011 Wiley-VCH Verlag GmbH & Co. KGaA, Weinheim)

elements from the periodic groups of II–VI or III–V with hundreds to thousands of atoms. They are typically synthesized from combinations of zinc(II), cadmium(II), selenide, and sulfide. QDs are famous for the quantum confinement effect, endowing them with unique size-dependent emission feature. In addition to tuning the emission wavelength of QDs by changing their size, engineered QDs with different materials can cover the spectral range from the ultraviolet to the infrared. In addition, QDs possess a lot of advantages including high photostability, strong luminescence with narrow and symmetric emission, size-tunable emission wavelength, large Stokes shift, good solution processibility, and versatile surface chemistry, which make QDs with a bright potential for NIR fluorescent imaging in vivo [36, 38, 45, 159, 160].

Most QDs applied for bioimaging are constructed with core/shell structures, where the nanocrystal core is usually coated with another material to protect and even enhance their optical properties. Meanwhile, to meet the requirement of in vivo imaging, QDs must have remarkable NIR emission, excellent biocompatibility, high photostability, and good water solubility. However, many of the existing QDs synthesized from hydrophobic conditions show water insolubility, preventing their

further bio-applications. Thus, hydrophilic modification is a vital step prior to the bioimaging application. To date, a variety of strategies developed to functionalize the hydrophobic QDs are focused on modifying their surfaces or constructing additional shells, including direct encapsulation by hydrophilic polymers, ligand exchange with hydrophilic ligands, and passivation of the QD surface. One useful approach for enhancing the dispersity of QDs in aqueous solution is the surface modification with anionic carboxylate groups. In addition, QDs with bright fluorescence and high quantum yields are important for their in vivo imaging application. QDs with narrow emission wavelength and high quantum yields are often obtained by solvothermal methods using organometallic precursors in nonpolar organic solvents. Due to the hydrophobic surface coating, QDs obtained from these methods require hydrophilic modifications for bioimaging purposes. 3-Mercaptopropionic acid-capped CdTe QDs emitted in the range 700–800 nm were prepared with microwave-assisted aqueous synthesis, and they were highly accumulated in the liver after intravenous injection. Although QDs can passively target tumorous sites in living mice resulted from EPR effect, the underlying targeting mechanism limits their applications to further distinguish tumors with different phenotypes. In this context, an active targeting strategy is important for the tumor detection by QDs [161].

Numerous methods have been developed to synthesize QDs directly in aqueous solution, since these hydrophilic QDs with lower toxicity might be more favorable for imaging in vivo. For instance, NIR Ag_2Se QDs with tunable fluorescence and low cytotoxicity were synthesized by using Na_2SeO_3, silver ions, and alanine at 90 °C in aqueous solution and subsequently used for bioimaging in living mice [163]. Moreover, such aqueous QDs with NIR emission were also employed for bioimaging in vivo with enhanced distribution, extended circulation time, and targeting tissue ability [162, 164, 165]. In another case, CdTe/CdS core/shell QDs with tunable NIR fluorescence were prepared in aqueous solution by a facile one-step method and showed high-sensitive imaging in targeted tumor sites in vivo [166]. Moreover, ultrasmall CdTe QDs with excellent water dispersibility and tunable NIR emission were synthesized by microwave method and successfully employed for tumor-targeting imaging in mice (Fig. 2.13) [162].

NIR QDs were also constructed to track the stem cells and labeled neutrophils to monitor their behavior inside living animals by noninvasive imaging [167]. For instance, due to minor autofluorescence of tissues in the second NIR region (NIR-II, 1.0–1.4 μm), Ag_2S QDs in NIR-II region were successfully used for dynamic monitoring of human mesenchymal stem cells (hMSCs) in vivo detectable of as few as 1000 cells [168]. The in situ translocation and dynamic distribution of transplanted hMSCs in the lung and liver can be detected up to 14 days with a high temporal resolution no more than 100 ms (Fig. 2.14).

In addition, NIR QDs were employed to stain the whole body of small animals with multiple color emission. For example, glutathione-coated QDs conjugated with glutathione S-transferase (GST) tagged luciferase were employed for whole-body fluorescence imaging in vivo [169]. Moreover, the sensitivity of NIR QDs was systematically investigated for in vivo imaging. Commercial Q-dot 800 QDs were

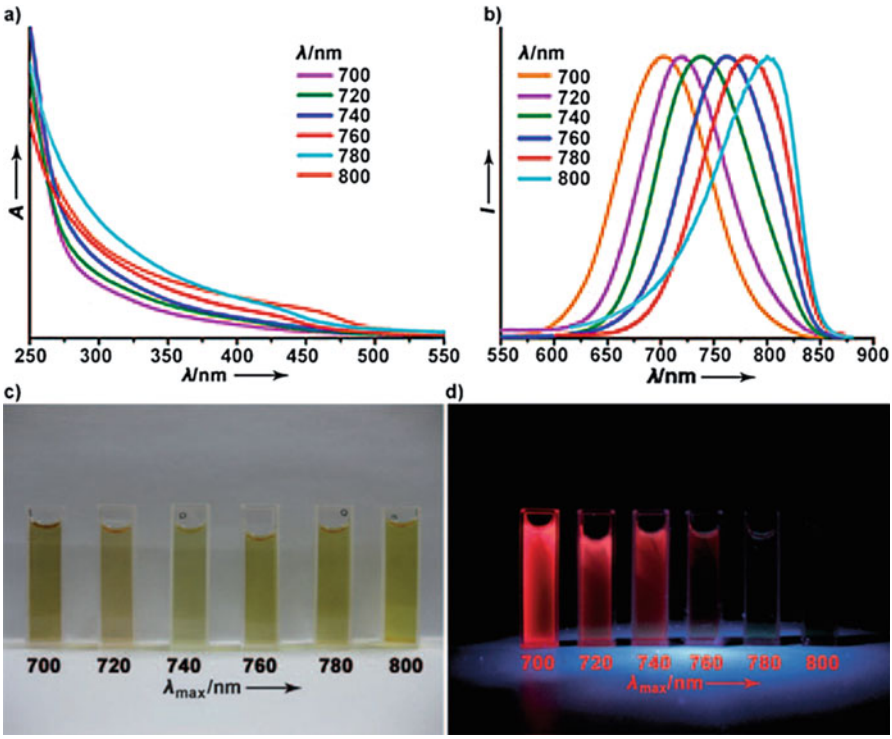

Fig. 2.13 (**a**) UV and (**b**) photoluminescence spectra of ultrasmall CdTe QDs with controllable emission in the range of 700–800 nm (λ excitation, 450 nm). Photographs of QDs in aqueous solution under (**c**) ambient light and (d) UV irradiation (λ excitation, 365 nm) [162] (Reprinted with permission from Ref. [162], Copyright 2011 Wiley-VCH Verlag GmbH & Co. KGaA, Weinheim)

conjugated with cell-penetrating peptides (CPPs) and subsequently employed to label oral carcinoma cells via endocytosis. Then, the QD-labeled cells were inoculated in several parts of nude mice in different amounts. The results displayed a sufficient signal with at least 104 QD-labeled cells, and the longest observable time extended to more than 16 days [170].

Multifunctional NIR fluorescence probes based on QDs were also developed for targeted tumor imaging in vivo [171]. Moreover, functionalized QDs have been widely explored for multimode bioimaging. Thus, it is important to develop suitable surface coatings to construct efficient QDs for bioimaging. In order to obtain functionalized QDs, a variety of surface coating methods have been applied, such as compact ligands [172], polymer immobilization [173], micellar encapsulation [174, 175], and polyethylene glycol (PEG) coating [176]. For instance, the Cerenkov luminescence of [^{64}Cu] $CuInS_2$/ZnS QDs, which were optimized by controlling the QD amount and ^{64}Cu radioactivity level, were successfully employed for in vivo tumor imaging [177]. Two-photon excitation technique is an attractive tool for in vivo tissue imaging, since it makes QD excitation in the NIR window with deep

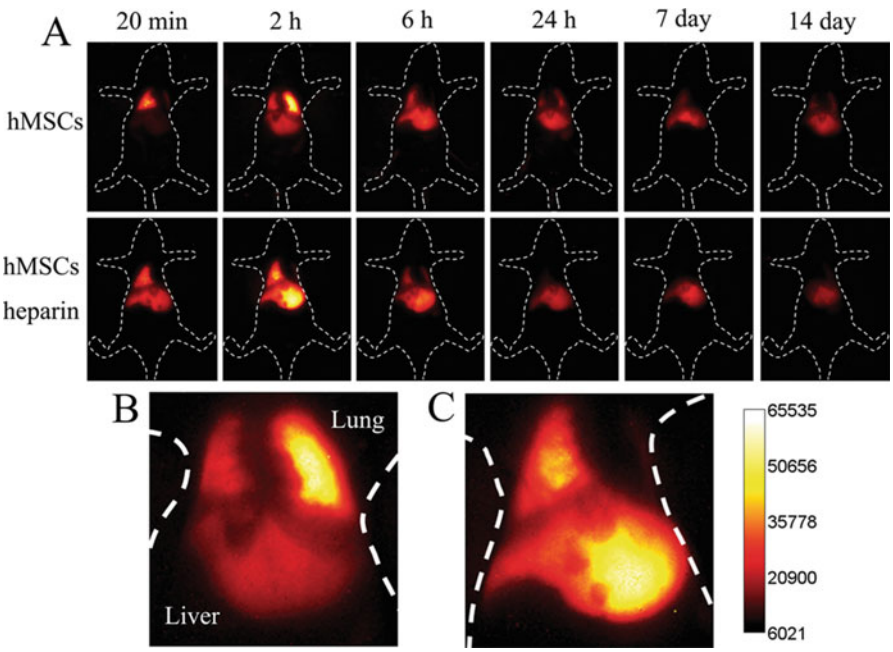

Fig. 2.14 (**a**–**c**) In vivo tracking of hMSCs via intravenous injection of Ag_2S QDs in mice [168] (Reprinted from Ref. [168], Copyright 2013 Wiley-VCH Verlag GmbH & Co. KGaA, Weinheim)

tissue penetration and negligible autofluorescence. Except for imaging QDs inside the tissue, they can also be applied for coating glass pipettes that are used to target visually identified neurons for electrophysiological studies. For example, glass pipettes coated with QDs that can exhibit excellent two-photon excitation signals were used for deep brain tissues imaging [178].

5.2.3 Carbon Dots

Carbon dots (C-dots), as fluorescent nanocarbons with sizes below 10 nm, are accidently discovered by purifying the single-walled carbon nanotubes (SWCNs) [179]. C-dots possess sp^2 character ascribed to three-dimensional nanocarbons, which are different from nanocrystalline graphite. Similar with traditional QDs, C-dots combine several favorable features such as size- and wavelength-dependent emissions, less photo-bleaching, and ease of bioconjugation. In addition, C-dots have many additional merits including easy preparation, low toxicity, easy excrement, weak protein adhesion, low disturbance by the immune system, and versatile surface chemistry. Due to the excellent photoluminescent properties and good biocompatibility, C-dots are attractive and eco-friendly candidates for bioimaging applications [46, 180–185].

Up to now, many strategies have been developed to produce C-dots in low cost and at a large scale [186–190]. Approaches for preparing C-dots can be usually classified into two categories: top-down and bottom-up approaches. Top-down

approaches for the fabrication of C-dots from prime materials like graphite powder or multi-walled carbon nanotubes (MWCNs) are generally executed under severe physical or chemical conditions such as laser ablation, arc discharge, and electrochemical oxidation [191]. Generally, C-dots obtained by laser ablating method are not fluorescent, but the surface passivation could substantially enhance their fluorescence intensity. Bottom-up approaches usually employ molecular precursors such as glucose and fructose with external energy source including ultrasonication, microwave pyrolysis, and heating. Typically, the surfaces of raw materials are oxidized by nitric acid (HNO_3) and then purified by separation processes such as centrifugation, dialysis, and electrophoresis. Besides, C-dots prepared by hybrid strategies combining elaborate functionalization with mild carbonization processing may show distinct surface functionalities.

Due to abundant carboxylic acid moieties spreading on the surface, C-dots possess sufficient water solubility and are facile to be functionalized with a variety of organic, inorganic, polymeric, and biological species. Moreover, C-dots possess great advantages including nearly isotropic shapes, ultrafine dimensions, tunable surface functionalities, as well as simple and cheap synthesis, making them highly potential in fluorescent bioimaging. However, pure C-dots are generally not fluorescent and do not display biofunction because of their poor interaction with biological species. Thus, it is important to engineer the functional surface of C-dots with tailored biological coatings for improving the fluorescence intensity [192].

Fluorescent C-dots are usually water-soluble with high photostability and good stability [193]. For instance, C-dots obtained from the passivation of commercial lampblack can be stored for up to 6 months [194]. Meanwhile, systematic cytotoxicity evaluations demonstrated that both raw C-dots and passivated C-dots exhibited low cytotoxicity at the concentration required for fluorescence bioimaging [182]. Thus, to meet the imaging application in vivo, it is important to engineer the surface functionality of C-dots with NIR emission, high quantum yield, excellent biocompatibility, and durable photostability [6].

NIR fluorescent C-dots, deemed as benign nanoprobes, have attracted great attention for imaging in vivo. It is necessary to understand the in vivo kinetic behavior of these particles which is required for clinical translation. For instance, C-dot-ZW800 conjugate was prepared by coupling C-dots with NIR dye ZW800, to monitor the in vivo kinetic behavior and the effect of tumor uptake via three injection routes: intravenous (i.v.), subcutaneous (s.c.), and intramuscular (i.m.) routes. The C-dot-ZW800 conjugate showed high photostability and rapid renal clearance with relatively low retention in the reticuloendothelial system and displayed effective passive tumor-targeted imaging with high tumor-to-background contrast (Fig. 2.15) [195].

Great efforts have been made to tailor C-dots for targeting tumors in vivo. For instance, photosensitizer-conjugated C-dots (C-dots-Ce_6) possessing excellent imaging and tumor-homing ability were successfully developed, showing simultaneous enhanced NIR fluorescence imaging and remarkable photodynamic efficacy of gastric cancer tumor in vivo (Fig. 2.16) [196]. In addition, C-dot-based hybrid nanosystems can also be used for in vivo determination of various biologically

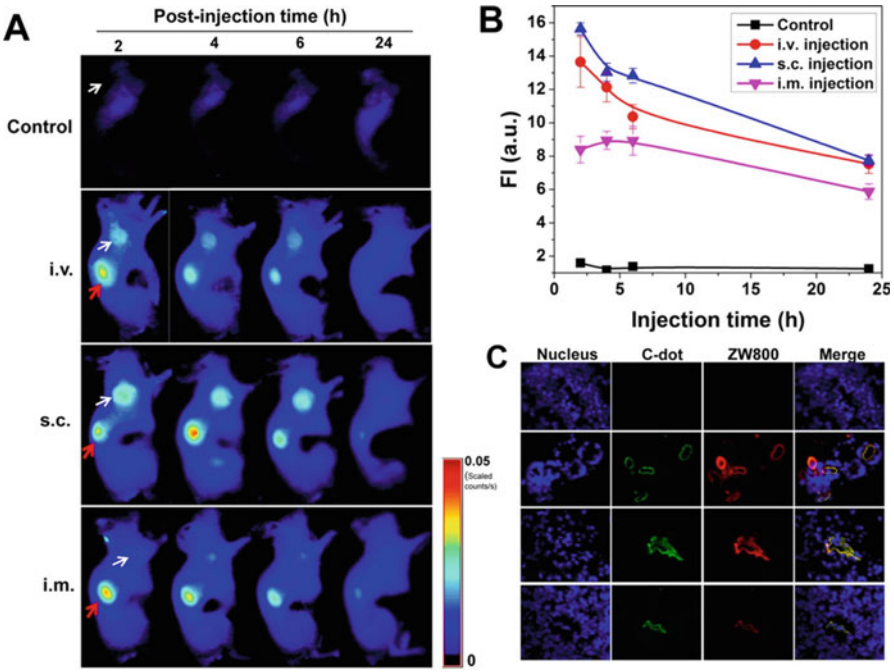

Fig. 2.15 (**a**) NIR fluorescence images of SCC-7 tumor-bearing mice obtained at different time points: control (without injection), i.v. injection, s.c. injection, and i.m. injection (white arrow points to tumor; red arrow points to the kidney). (**b**) Tumor region-of-interest analysis. (**c**) Ex vivo fluorescence images obtained to demonstrate tumor uptake of the nanoparticle conjugate [195] (Reprinted from Ref. [195], Copyright 2013 the American Chemical Society)

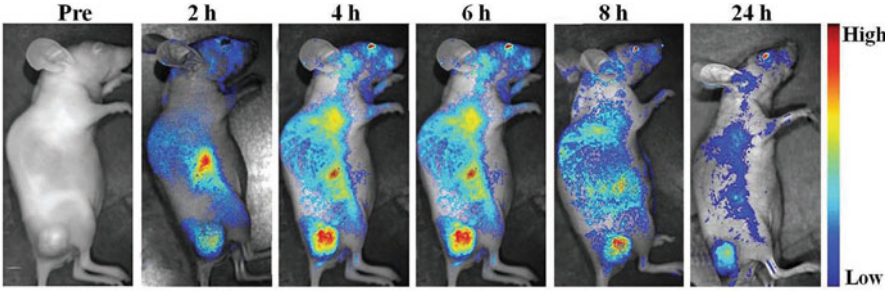

Fig. 2.16 Real-time in vivo NIR fluorescence images of intravenously injected C-dots-Ce_6 in nude mice upon time [196] (Reprinted from Ref. [196], Copyright 2012 Wiley-VCH Verlag GmbH & Co. KGaA, Weinheim)

relevant species. For example, C-dot-based two-photon fluorescent probe has been applied for imaging and biosensing of pH gradients in living tissues at depths of 65–185 μm without the interference resulted from other biological species [197].

Intravenous injection plays a vital role in the study of pharmacokinetics, biodistribution, and toxicological evaluations of C-dots. Due to the small size and high solubility, C-dots can be excreted efficiently via urine with negligible accumulation in the internal organs. For example, polymer-coated nitrogen-doped C-dots with diameters of 5–15 nm were prepared by solvothermal reaction for tumor-targeted imaging in vivo. The C-dot-based nanosystem was intravenously injected into glioma-bearing mice, displaying an enhanced accumulation within the glioma based on the EPR effect [185].

5.2.4 Carbon Nanotubes

Carbon nanotubes (CNTs) with a unique one-dimensional structure and inherently physical, mechanical, and chemical properties are classified into two structural forms: SWNTs and MWNTs [198]. In general, CNTs display NIR fluorescence with relatively low quantum yield and exhibit excellent resistance to photobleaching and low cytotoxicity.

The bandgap between each semiconducting SWNT is in the order of 1 eV, which allows for the fluorescence located in the NIR-II (900–1600 nm) region upon NIR-I excitation [199]. Furthermore, the large Stokes shift between the excitation at 550–850 nm and emission at 900–1600 nm would substantially reduce the autofluorescence resulted from biological tissues during bioimaging, providing enhanced imaging sensitivity. Despite the encouraging properties of SWNTs with NIR fluorescence, the low quantum yield of SWNTs is the main obstacle for further in vivo imaging applications. It has been demonstrated that the photoluminescence quantum yield is closely related to the length and surface coating of CNTs. Thus, the coating exchange approach can effectively enhance the quantum yield of SWCNTs, and the resulted bright fluorescence can directly visualize the small tumor vessels beneath the thick skin [200]. Enhanced fluorescence of SWNTs was also obtained from the modification with gold that shortened radioactive lifetime through resonance coupling of SWNT emission to plasmonic modes in the metal [201].

CNTs can be synthesized by various approaches including laser ablation, arc discharge, and chemical vapor deposition (CVD) [202]. Generally, CNTs obtained by laser ablation produces are clean but accompanied by relatively low yield. In contrast to laser ablation, arc discharge can produce larger quantities of CNTs but with poor purity. In contrast to arc discharge and laser ablation, CVD is relatively a mild approach for the production of CNTs with lower operated temperature and good scalability. However, MWNTs or SWNTs obtained from traditional CVD processes always show large diameter distribution and poor quality. Thus, more advanced and facile strategies for CNT production are highly desirable. Generally, the purification of SWNTs includes removing the structural impurities generated during the synthesis process and screening out SWNTs with homogeneous size distribution. Commonly used purifying techniques include acid treatment, oxidation, cutting, ferromagnetic separation, annealing, microfiltration, ultrasonication, functionalization, ultracentrifugation, and chromatographic separation.

A research advance involves the use of SWNTs as NIR-II fluorescent imaging agents [203–209]. A great number of fundamental and biological studies using CNTs

showed excitation bands ranging from 600 to 800 nm and emission bands at the range of 950–1300 nm. Fluorescent imaging in the NIR-II window holds high promise on account of minimal autofluorescence and tissue scattering. For instance, high-frame-rate video in vivo imaging can be visually observed by intravenously injecting SWNTs into mice. Compared with the conventional NIR-I window (700–900 nm) by indocyanine green, SWNTs displayed much longer remain of feature contrast and integrity with increasing feature depth by tissue phantom studies. By combining with principal component analysis (PCA), NIR-II fluorescence imaging may become a powerful way to image deep tissues with high resolution, which is useful for a wide range of applications from bioimaging to disease diagnosis [210].

Generally speaking, SWNTs used for bioimaging applications are a complex mixture of semiconducting and metallic species with random chirality, which greatly prevent simultaneous resonant excitation of all CNTs and strongly decrease the emission at a single well-defined wavelength. Based on the structure-dependent interaction of SWNTs with an allyl dextran size-exclusion gel, brightly fluorescent SWNTs consisting of predominantly (12,1) and (11,3) chirality were successfully produced and achieved for real-time NIR-II fluorescence imaging of deep organs with high-magnification imaging of hind limb vessel in mice (Fig. 2.17) [211].

To meet the requirement of cancer imaging, contrast agents should be selectively accumulated in the tumor area rather than distributions in healthy tissues. For instance, polymer-functionalized SWNTs were successfully used to achieve ultra-high accumulation in tumors with long blood circulation in vivo (Fig. 2.18) [212]. Based on the intrinsic NIR-II fluorescence of SWNTs, both video-rate imaging and dynamic contrast imaging of tumors were performed through PCA. The fluorescent imaging showed unambiguous tumor identification up to 72 h after the injection. In addition, the 3D reconstruction of SWNT distribution revealed highly passive tumor uptake of SWNTs that mainly resulted from the EPR effect. In addition, fluorescent SWNTs engineered with multifunctional M13 phage were successfully achieved for targeted fluorescence imaging of tumors, showing a great potential for specific diagnosis and therapy monitoring of hard-to-detect areas [213].

5.2.5 Graphene-Based Nanomaterials

Graphene-based nanomaterials include graphene, graphene oxide (GO), reduced graphene oxide (rGO), graphene quantum dots (GQDs), and their derivatives. Graphene, an atomically thick sheet of two-dimensional honeycomb monolayer, is the basic building block for all other dimensionalities of carbon nanomaterials, such as CNTs, fullerene, and carbon nanohorns. GO is a highly oxidized form of chemically modified graphene, which comprises of single atom thick layer of graphene sheets with hydroxyl (-OH) and epoxide (-O-) functional groups on the two accessible sides and carboxylic acid (-COOH) groups at the edges. By the reduction treatment of GO, the oxygen content, surface charge, and hydrophilicity of GO are decreased, and then rGO is produced with restored electrical conductivity and enhanced optical absorbance. GQDs are two-dimensional graphene fragments

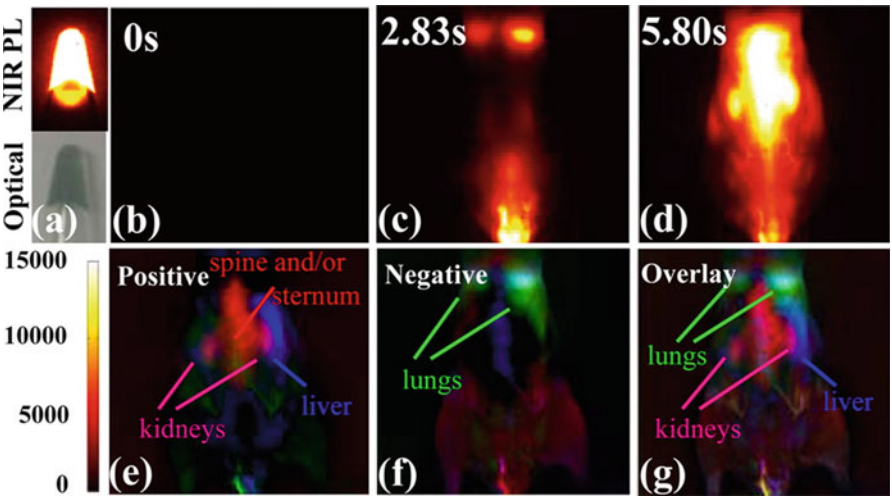

Fig. 2.17 (**a**) Optical and fluorescence images of (12,1) and (11,3) SWNT solution. (**b**) Initial NIR-II fluorescence image of nude mouse without the injection of SWNTs. (**c**, **d**) NIR-II fluorescence images after the injection of SWNTs with different time. (**e**–**g**) PCA images of positive, negative, and overlaid components. Green represents lungs, pink represents kidneys, and blue represents the liver [211] (Reprinted from Ref. [211], Copyright 2012 the American Chemical Society)

sized in 10–60 nm, usually not single-layer but multilayers (~10 layers of rGO). On account of their versatile surface functionalization and ultrahigh surface area, graphene and its derivatives can be easily functionalized by small molecular dyes, polymers, nanoparticles, drugs, or biomolecules to obtain graphene-based nanomaterials for various biomedical applications. Due to intrinsic optical properties in the visible and NIR spectral region, low cytotoxicity, intrinsic aqueous solubility, and versatile surface functionalization, graphene-based nanomaterials have attracted considerable interest for bioimaging [4, 11, 23, 42, 53, 214–218].

Graphene can be synthesized by either bottom-up or top-down strategy [219]. The bottom-up strategy mainly includes CVD, organic synthesis, and solvothermal synthesis [217]. The top-down strategy mainly involves mechanical, physical, and chemical exfoliation methods [220]. GO is typically produced by the Hummers' method through the oxidative exfoliation of graphite using $KMnO_4$/H_2SO_4. rGO can be obtained by treating GO with reducing agents, such as hydrazine, hydrazine hydrate, *L*-ascorbic acid, and so on [221]. GQDs are usually prepared by thermal oxidation of GO or other carbon precursors [11, 214].

Compared with classical QDs, GQDs have merits of low cytotoxicity, good biocompatibility, and physiological solubility and can be used directly for bioimaging without further surface functionalization or processing. In addition, GQDs have unique optical properties of upconversion fluorescence and pH dependence, which make them suitable for safe and efficient bioimaging [223]. To eliminate the autofluorescence interference of biological tissues, lots of efforts have been

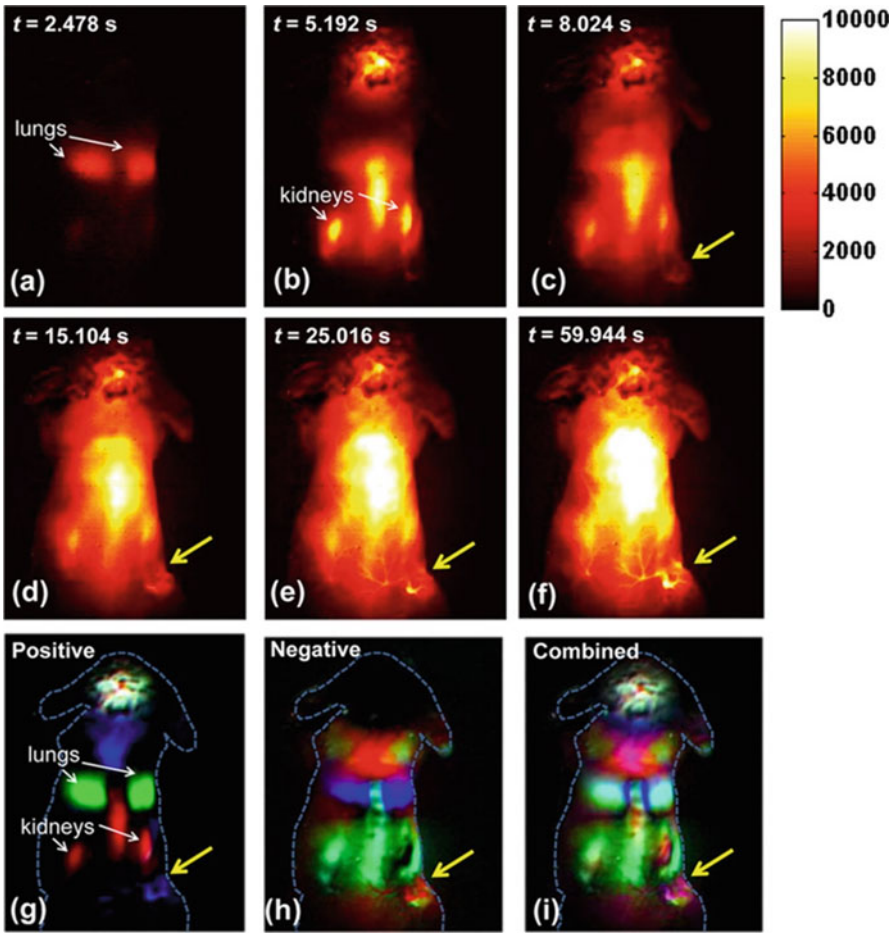

Fig. 2.18 (**a**–**i**) NIR-II fluorescence images and dynamic contrast-improved images using polymer-functionalized SWNTs based on PCA analysis. Yellow arrows indicate the tumor [212] (Reprinted from Ref. [212], Copyright 2012 the American Chemical Society)

expended in constructing NIR fluorescent GQDs for imaging in vivo [222]. For example, NIR graphene nanoparticles (GNPs) were synthesized from carbon fibers through a simple reaction. Due to the excellent biocompatibility, sufficient water solubility, and high luminescence stability, GNPs were proven to be greatly attractive NIR fluorescence probes for high-contrast bioimaging of deep tissues and organs (Fig. 2.19) [222]. In addition, GQDs with bright fluorescence emission around 815 nm were synthesized by one-step pyrolysis of *L*-glutamic acid and subsequently used to image biological targets in vivo with high sensitivity due to their large Stokes shift of 455 nm [224].

By taking advantage of photostable, nontoxic, and easy conjugation properties, GQDs can also be designed and applied for in situ drug delivery and imaging. For

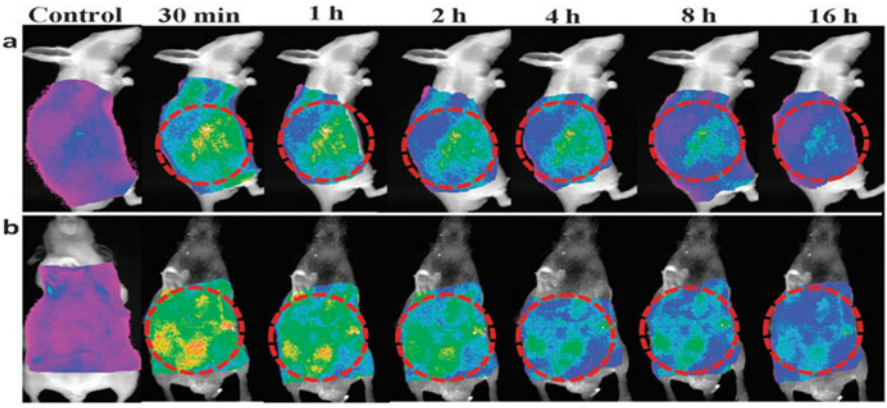

Fig. 2.19 (**a**) Side and (**b**) front view fluorescent images of mice using GNPs [222] (Reprinted from Ref. [222], Copyright 2013 the Royal Society of Chemistry)

example, biodegradable polymers, such as hyaluronic acid (HA), were selected as linkage groups for loading fluorescent species onto the surfaces of GQDs. The obtained GQD-HA composites were demonstrated as efficient targeting agents to achieve specific targeted delivery, since the tumor tissues showed more brighter fluorescence during the investigation of in vivo biodistribution in mice [225].

Two-photon fluorescent probes with bright photoluminescence are highly desirable to be able to visualize biological activities with high spatial resolution, deep tissue penetration inside living organisms, low autofluorescence, and minor photodamage. For example, nitrogen-doped graphene quantum dots (N-GQDs), obtained from a facile solvothermal method, were used as efficient two-photon fluorescent probes for deep tissue imaging [226]. The obtained N-GQDs displayed high two-photon absorption cross section, large imaging depth, and outstanding photostability. In addition, another feasible approach to improve the in vivo imaging performance in complex biological conditions is introducing a two-photon dye (TP dye) as the signal reporter. For instance, by the combination of GO with the two-photon excitation (TPE) technique, a GO/aptamer-TP dye conjugate was successfully constructed and achieved for in vivo imaging of ATP with high sensitivity and selectivity [59]. In another case, GO nanoparticles grafted with PEG polymer were injected into mouse body from the tail vein, the flow and distributions of GO nanoparticles in blood vessels can be clearly observed by using a deep-penetrating two-photon imaging technique, and the imaging depth could reach 300 μm or more (Fig. 2.20) [227].

For practical NIR imaging using functional graphene nanomaterials, real-time imaging of in vivo photo absorber distribution and monitoring of posttreatment therapeutic outcome are vital to optimize personalized cancer treatment. The development of multifunctional probes combined with therapeutic functions and imaging capabilities thus becomes important. For example, rGO-IONP-PEG, prepared from

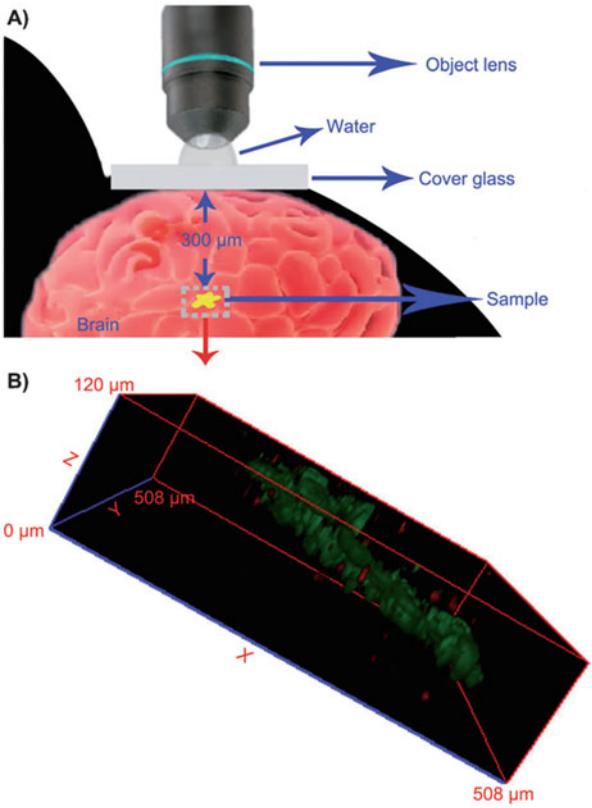

Fig. 2.20 (**a**) Two-photon luminescence microscopy and corresponding image of GO-PEG nanoparticles in a mouse brain. (**b**) A reconstructed image illustrating the three-dimensional distribution of GO-PEG nanoparticles in vivo [227] (Reprinted from Ref. [227], Copyright 2012 Wiley-VCH Verlag GmbH & Co. KGaA, Weinheim)

rGO-iron oxide hybrid nanoparticles (rGO-IONP) with PEG modification, was successfully employed for tumor imaging in vivo and triple modal imaging-guided photothermal therapy for cancer [228].

Moreover, graphene can also be developed as multifunctional nanomaterials in biomedical applications of bioimaging, diagnosis, and therapeutics. For instance, a multifunctional graphene (MFG) having water dispersible, fluorescent, and magnetic functions was developed through microwave-heated sonication-assisted method. The MFG was demonstrated as a useful in vivo imaging probe, which exhibited even distribution in whole zebra fish for in vivo imaging. Furthermore, taking advantage of the magnetic property, MFG could also be utilized in biomedical diagnostics [216]. By covalently grafting UCNPs with nanographene oxide (NGO) via bifunctional PEG and then loading phthalocyanine (ZnPc) on the surface of NGO, nanocomposites named UCNPs-NGO/ZnPc were formed. The obtained UCNPs-NGO/ZnPc can be applied not only for in vivo imaging with high contrast for diagnosis but also for generating singlet oxygen for photodynamic therapy. The nanosystem could also efficiently convert the 808 nm laser energy into thermal energy for photothermal therapy [229].

5.2.6 Nanodiamond

Fluorescent nanodiamond (FND) is an emerging nanomaterial based on sp^3-carbon for bioimaging and cell tracking [230]. FND possesses unique and well-established nitrogen-vacancy (NV) emission centers that endow it with excellent photostability and inherent biocompatibility [7, 32, 231]. NV has an absorption maximum at 550 nm, and when exposed to green-orange light, it emits bright fluorescence at 700 nm with a lifetime of more than 10 ns. In addition, the NV center is perfectly photostable without photo-bleaching and blinking and could be little affected by surface functionalization. Unlike other fluorescent nanoparticles that can be synthesized with wet chemistry methods, FND can be fabricated only by physicochemical means under extreme conditions. Together with facile surface modification on diamond nanoparticles, high sensitivity of NV centers endows these nanoparticles with unprecedented performance in bioimaging and long-term cell tracking, especially in stem cell research (Fig. 2.21) [7, 32, 34, 232, 233].

The unprecedented biocompatibility of FND was successfully evaluated and demonstrated by long-term imaging for *Caenorhabditis elegans* [234]. The toxicity assessments showed that the FND present in cells was stable and nontoxic and did not induce any change in longevity and reproductive potential of the worms. The outstanding photostability and excellent biocompatibility feature of FND enabled continuous imaging of the whole digestive system and monitoring of cellular and developmental processes of the living organism for several days.

However, to meet the requirement of practical imaging, some limitations such as weak brightness and tough bioconjugation have to be overcome. Chang et al. developed FND particles by utilizing nitrogen-rich type Ib diamonds, which showed high fluorescence and ready functionalization with proteins for cell imaging [235, 236]. Additionally, the surfaces of diamond nanostructures play an important role in determining the utility and biocompatibility of these nanostructures in biological and medical applications. The first step of diamond surface modification often involves harsh treatment with strong chemicals or plasma irradiation to introduce functional groups onto the surface. Once surface functional groups are established, various linker molecules or biomolecules, including biomarkers, therapeutic drugs, and genes, can be grafted onto the surface. The surface of diamond can be flexibly tuned through the surface modification methods such as oxidative treatment, halogenation, reduction, hydrogenation, and thiolation [237–239].

Based on the surface modifications of FND with various functional groups, including targeted probes and drugs, a multifunctional platform for combined targeting, imaging, and therapy using diamond nanoparticles was demonstrated. This combination allows simultaneous diagnosis and therapy and also enables monitoring therapeutic delivery, transport, and response. In addition, FND is chemically inert and does not release toxic chemicals even in harsh environments. Thus, these properties endow diamond nanostructures with intrinsic biocompatibility. Thanks to their inherent photochemical and chemical inertness and their emission in the NIR region, FND has been widely employed for in vivo imaging and long-term tracking as cellular biomarkers [230, 237]. For instance, FND-based platforms can be used for long-term imaging without eliminating in vivo cell migration and

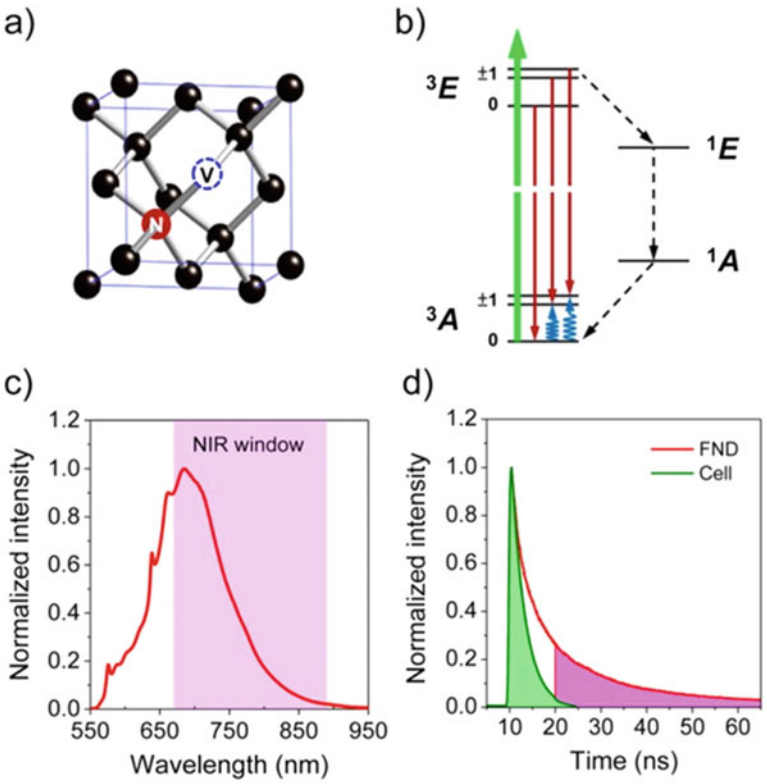

Fig. 2.21 (**a**) Structure and (**b**) energy level diagram of the NV center in diamond. The red sphere, blue dashed circle, and black spheres in (**a**) denote nitrogen, vacancy, and carbon atoms, respectively. The green, red, and blue sinusoidal and black dashed arrows in (**b**) denote optical excitation, fluorescence emission, microwave excitation, and intersystem crossing relaxation, respectively. (**c**) Comparison between the fluorescence spectrum of FND excited with a 532 nm laser and the NIR window of biological tissue. (**d**) Comparison between the fluorescence lifetime of FND in water and endogenous fluorophores in cells. Time gating at 10 ns is indicated for background-free detection [7] (Reprinted from Ref. [7], Copyright 2016 the American Chemical Society)

differentiation into type I and type II pneumocytes. Moreover, by using the combined technology of FND labeling, FLIM, and fluorescence-activated cell sorting (FACS), researchers can unequivocally monitor and identify the transplanted $CD45^{-}CD54^{+}CD157^{+}$ lung stem/progenitor cells in vivo under single-cell resolution and further quantify their engraftment and regenerative capabilities over a week (Fig. 2.22) [233].

In order to meet some demanding bioimaging applications and to integrate with existing advanced protein labeling technologies, there is a need to reduce the particle size down to at least 10 nm. FND performs in vivo tracking of cells with good sensitivity, resolution, and precision. The fluorescence intensity of NV centers sensitively depends on the ground-state spin configuration that can be tuned by

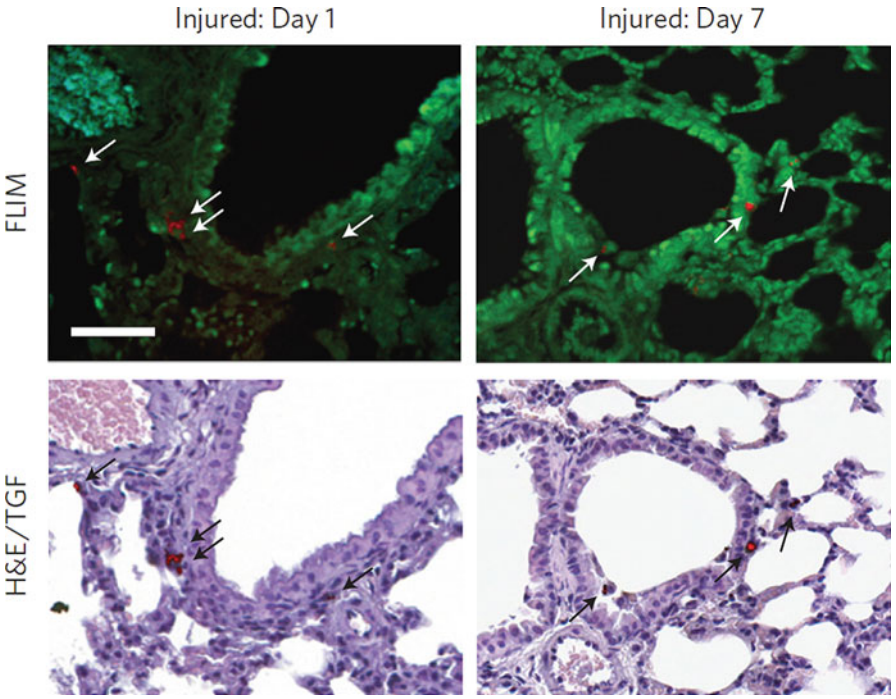

Fig. 2.22 FLIM, transforming growth factor (TGF) and corresponding bright-field hematoxylin and eosin (H&E) staining images of lung tissues using FND. White and black arrows indicate the FND-labeled lung stem/progenitor cells [233] (Reprinted from Ref. [233], Copyright 2013 Nature Publishing Group)

electron-spin magnetic resonance. By means of real-time selective fluorescence imaging of NV centers, successful long-term monitoring of a single nanodiamond in both *Caenorhabditis elegans* and mice was conducted, with extraordinary imaging contrast even in the presence of strong background autofluorescence [240].

Due to the excellent photostability and nontoxicity, FND was used as photostable labels and tracers for the intercellular transport of proteins. For example, FND coated with yolk lipoprotein complexes was successfully microinjected into intestinal cells to monitor the transportation of fat molecules and cholesterol in vivo. The results indicate that FND can be used as a safe and efficient nanocarrier for biomolecules without obviously changing the functionality of the cargos for cell-specific targeting, intercellular transport, and long-term in vivo imaging applications [232].

5.2.7 Upconversion Nanoparticles

UCNPs, featured as upconversion luminescence (UCL), are a unique class of lanthanide-doped nanoparticles with fluorescence emission upon NIR light excitation. UCL is a process where low-energy NIR light is converted to higher-energy light through the sequential absorption of multiple photons or energy transfers. Most

UCNPs consist of hexagonal $NaYF_4$ nanocrystals doped with trivalent lanthanide ions such as Er^{3+}, Yb^{3+}, or Tm^{3+}. Usually, UCNPs display multiphoton emission, and the peak wavelengths depend on the lanthanide dopant used. The size of UCNPs highly affects the quantum yields and is widely tunable in the range of 10–100 nm. Unlike in the case of C-dots, the emission wavelength of UCNPs is independent of the excitation wavelength. Remarkably, the quantum yields of UCNPs depend on both the power density of the laser and the particle size.

Compared with conventional contrast agents with downconversion, UCNPs possess a lot of merits as bioimaging probes: minimal autofluorescence, deeper penetration depth, less photodamage, hardly attacked by the immune system, narrow emission bands, tunable emission, no photo-bleaching, long luminescence lifetime at micro- to milliseconds scale, low toxicity to living systems, high cell permeability, and excellent chemical and physical stability. Due to their superior optical and chemical properties, UNCPs have been deemed as perfect fluorescent contrast agents for NIR imaging in vivo.

To use UCNPs as successful fluorescent labels, some major requirements must be met. Firstly, suitable size and uniform shape are the prerequisites for bioimaging [241]. Up to now, a number of approaches and considerable research efforts have been devoted to preparing UCNPs with different shapes and tunable sizes from 10 nm to sub-mm. Thermal decomposition and hydro(solvo)thermal synthesis are the two most common approaches for the production of uniform hydrophobic nanocrystals [242]. A variety of UCNPs with monodispersed size and uniform shapes have been successfully prepared by the modified thermal decomposition method [243, 244]. For instance, monodispersed $NaYF_4$:Yb^{3+}/Tm^{3+} nanocrystals with enhanced NIR-to-NIR upconversion photoluminescence were successfully synthesized by using a modified co-thermolysis method [241]. Unlike in the case using thermal decomposition method, highly crystalline materials can be prepared by hydro(solvo)thermal approach at much lower temperature and without the requirement of annealing process. However, the UCNPs synthesized by thermal decomposition and hydro(solvo)thermal approach are hydrophobic. Since the UCNPs as biological fluorescent probes should be water-soluble, a facile surface modification or functionalization is needed to convert hydrophobic UCNPs into hydrophilic ones for bioimaging applications. Currently, many surface modification strategies have been developed to convert the hydrophobic UCNPs into water-soluble ones. These methods include ligand exchange, cation-assisted ligand assembly, organic ligand-free synthesis, ligand oxidation reaction, layer-by-layer method, hydrophobic-hydrophobic interaction, host-guest interaction, and silanization. Generally, UCNPs processed by ligand exchange have no obvious changes for their morphology, crystallization, and chemical properties. Similarly, UCNPs treated by the ligand oxidation process also show no obvious adverse effects on the morphology and luminescence properties. Cation-assisted ligand assembly is also an efficient way to convert UCNPs into water-soluble ones. For example, oleylamine (OM)-coated $NaYF_4$:Yb,Er/Tm UCNPs are hydrophobic and can be converted into water-soluble system by cleaving OM along with the cation exchange. By taking advantage of hydrophobic-hydrophobic interaction, hydrophobic UCNPs can be converted

into hydrophilic forms by coating hydrophilic small molecules or polymers [245, 246]. Moreover, hydrophilic ligands can be linked on the surface of hydrophobic nanoparticles mediated by host-guest interactions [247]. For instance, oleic acid (OA)-coated $NaYF_4$:Yb,Er/Tm nanoparticles were successfully transferred into water-soluble forms via the robust host-guest interaction between α-cyclodextrin (α-CD) and OA [248]. The size of nanoparticles can be remained on account of hydrophobic-hydrophobic interaction and host-guest interaction. In addition, silanization is a powerful and popular tool for the surface functionalization of nanoparticles on account of high biocompatibility of silica, and silica-coated UCNPs were employed for bioimaging. Both hydrophilic and hydrophobic UCNPs can be modified with silica coating. For UCNPs with hydrophobic ligands, reverse micro-emulsion method is often employed to conduct silica coatings [249, 250], while UCNPs with hydrophilic ligands can be modified by the Stöber method [251]. Among the abovementioned surface treatment strategies, silanization is the only inorganic modification approach, offering a core/shell structure and inducing $–NH_2$, –COOH, or –SH groups for further bioconjugation. However, the sizes of UCNPs are often enlarged by the silanization.

To simplify the procedure of synthesis and posttreatment, a variety of one-step synthetic strategies [252], including polyol process assisted by hydrophilic ligands [253], hydrothermal route assisted by binary cooperative ligands (HR-BCL) [254], and ionic liquid-based synthesis [255], were used to prepare water-soluble UCNPs. In general, the one-step synthetic method can greatly simplify the procedure of reaction and posttreatment. However, UCNPs with small and uniform sizes are hardly obtained. Although usually requiring complicated posttreatment, two-step approaches are convenient for tuning the size, shape, and crystallinity of UCNPs. In short, both one-step and two-step methods for converting the hydrophobic UCNPs into hydrophilic forms are under active developments.

The application of UCNPs in fluorescence imaging of tissues and living subjects has attracted increasing attention. Unquestionably, great research progress has been achieved in the development of uniform, ultrasmall-sized, water-soluble, and surface-functionalized UCNPs with multiplexed colors and high quantum yield. However, only few UCNP examples could thoroughly meet all the requirements for in vivo imaging. There are still many challenges to synthesize UCNPs with controllable size, hydrophilic properties, and biofunctionality as fluorescence probes for in vivo imaging. To date, $NaYF_4$:Yb,Tm nanoparticles with a diameter of 11.5 nm are the smallest UCNPs obtained from solvothermal method and coated with polyacrylic acid (PAA) [256]. These hexagonal $NaYF_4$:Yb,Tm nanoparticles were successfully used for the long-term tracking of the biodistribution in vivo.

Some UCNPs are ideally suited for in vivo fluorescent bioimaging due to their merits of NIR-to-NIR upconversion. For example, core/shell α-$NaYbF_4$:Tm^{3+}/CaF_2 nanoparticles exhibited highly efficient NIR emission at ~800 nm when excited at ~980 nm, which enabled their applications for high-contrast deep tissue bioimaging [257]. However, the 980 nm laser, typically employed to trigger the upconversion process, is highly absorbed by water in biological structures and could induce severe

overheating effect. To address the issue of NIR laser-induced tissue damage, Nd^{3+} ion was introduced as NIR absorber and sensitizer in conventional Yb^{3+}-doped UCNPs [258]. The integrated $Nd^{3+} \rightarrow Yb^{3+}$ energy transfer to conventional Yb^{3+}-sensitized upconversion processes is a versatile method to extend the single NIR excitation band of Yb^{3+} to shorter wavelengths. The excited band at 808 nm could offer high upconversion excitation efficiency similar to that of 980 nm excitation, while having substantially minimized tissue overheating effect. A similar approach was proposed to excite UCNPs by using 915 nm laser light, which showed the depth range in vivo imaging [259].

UCNPs, featured with distinct narrow emissions, are deemed as good color markers to simultaneously trace different biochemical species and monitor multiple organs [260]. For instance, UCNP-dye complexes based on $NaYF_4$ nanocrystals were synthesized by simultaneously modifying with amphiphilic polymer and fluorescent dyes via physical adsorption. The obtained supramolecular UCNP-dye complexes exhibited controllable visible emission spectra ascribing to the luminescence resonance energy transfer (LRET) from UCNPs to the organic dyes upon NIR excitation and achieved multicolor UCL imaging in vivo (Fig. 2.23) [261].

Targeted monitoring and bioimaging of special chemicals in biological systems are important, since these molecules or ions often play an important role in organisms. For example, efficient and sensitive monitoring of methylmercury ($MeHg^+$) in vivo is of great importance, because a certain amount of methylmercury accumulated in the organs of animals would result in prenatal nervous system and visceral damage. Considering the superior UCL of UCNPs, cyanine dye-assembled UCNPs were synthesized for UCL sensing and bioimaging of $MeHg^+$ in vivo (Fig. 2.24) [262]. The cyanine dye hCy7, a $MeHg^+$-sensitive dye, was loaded on the surface of lanthanide UCNPs, achieving the monitoring of $MeHg^+$ in vivo with high sensitivity. Moreover, targeted tumor imaging is also important for tumor diagnosis and therapy. This target-specific recognition includes ligand-acceptor and antigen-antibody interactions. For instance, recombinant chlorotoxin-mediated $NaYF_4$:Yb,Er/Ce UCNPs showed highly specific binding of tumors and can be used to directly visualize tumors in living mice with high-contrast images [263].

Common approaches to study the deep tissue imaging of most UCNPs mainly rely on direct injection of abundant UCNPs into tissue or special site of animals, which may cause long-term biosafety issues. Thus, an advanced approach is to develop highly sensitive UCNP-based fluorescence probes for in vivo imaging. UCNP-labeled cells delivered into injured muscles would undoubtedly offer useful insights for real-time monitoring of the myoblast transplantation therapy [261]. For example, sub-10 nm Gd^{3+}-doped $NaLuF_4$ UCNPs, synthesized via thermal decomposition, were effectively used with tracking limits of 50 and 1000 UCNP-labeled cells via subcutaneous and intravenous injection, where high-contrast UCL whole-body imaging of a black mouse with a penetration depth of ~2 cm was achieved [264].

In addition, the spatiotemporal regulation of light-gated ion channels is a useful tool to study physiological pathways and develop personalized theranostic

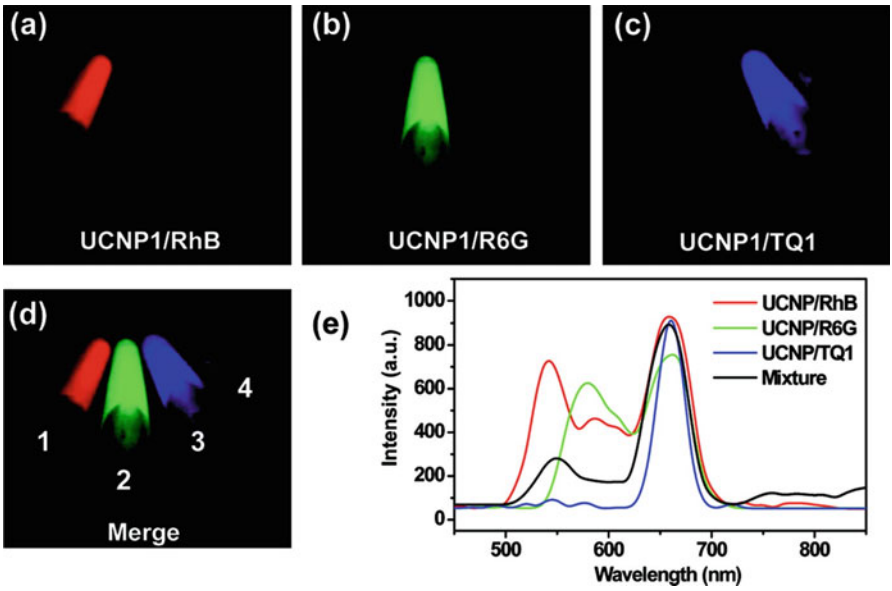

Fig. 2.23 (**a**–**e**) Multicolor UCL imaging of UCNP-dye complexes [261] (Reprinted from Ref. [261], Copyright 2011 the American Chemical Society)

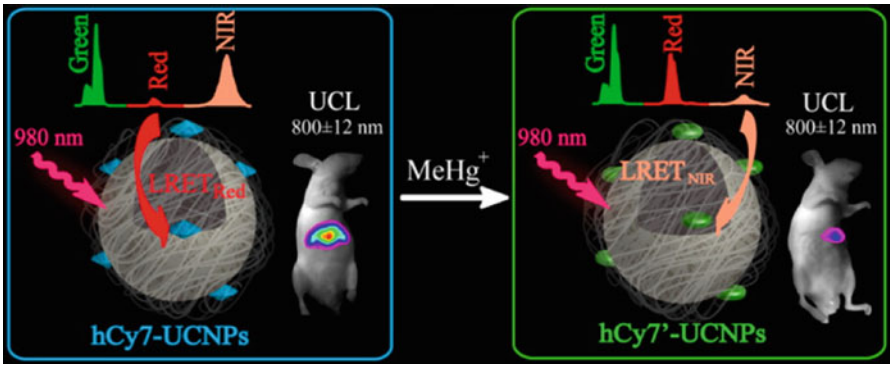

Fig. 2.24 Schematic layout of cyanine-modified UCNPs for in vivo imaging of methylmercury [262] (Reprinted from Ref. [262], Copyright 2013 the American Chemical Society)

modalities. Recently, a simple strategy based on native metabolic glyco-biosynthesis was used to achieve site-specific covalent localization of NIR light-responsive UCNPs on the cell surface through a copper-free click reaction under living conditions. Upon 808 nm light irradiation, the blue emission (at 480 nm) from UCNPs could remotely activate the photosensitive ion channel and effectively manipulate the cation influx in living zebra fish [265].

5.2.8 Noble Metal Nanoclusters

Noble metal nanoclusters (NCs), as a new type of luminescent nanomaterials, have been attracting extensive interest due to convenient surface bioconjugation and unique optical properties [266]. NCs are composed of a few to hundred atoms, and typically have diameters below 2 nm, making their dimensions between metal atoms and small nanoparticles. Since their sizes are close to the Fermi wavelength of electrons, NCs possess molecule-like properties such as discrete electronic states and size-dependent fluorescence [267]. Therefore, NCs are referred as fluorescent noble metal QDs. NCs have several distinct features including strong photoluminescence, good photostability, and large Stokes shift. To date, water-soluble NCs with different ligands and tunable emission have been developed in various biocompatible scaffolds, enabling them as useful fluorescence probes for bioimaging applications [268–275].

Various methods have been employed to prepare metal NCs with considerable quantum yield and sufficient brightness for the applications of bioimaging. However, NCs obtained from the reduction of metal ions tend to aggregate into large nanoparticles in aqueous solution. In addition, the emission properties of NCs can be easily affected by the ligands capped on the particle surface. Therefore, a judicious choice of capable agents or stabilizers is vital to obtain small metal NCs with high stability and enhanced fluorescence.

Thiol-containing small molecules are the most commonly used stabilizers in metal nanoparticle production due to the strong interaction between thiols and Au/Ag. For instance, glutathione as an excellent stabilizer was widely used to synthesize Au NCs with visible luminescence through the reduction of Au^{3+} with sodium borohydride ($NaBH_4$). Except for glutathione, a variety of thiols including tiopronin, thiolated cyclodextrin, phenylethylthiolate, and 3-mercaptopropionic acid are also good stabilizers and have been used for the preparation of metal NCs [267]. In addition, fluorescent metal NCs can also be prepared by etching large Au nanoparticles with thiols or capping agents, such as mercaptosuccinic acid. On account of their capability of sequestering metal ions from solution, both dendrimers and polymers with a mass of carboxylic acid groups were used as templates to produce metal NCs. Biomacromolecules such as DNA, peptides, and proteins were also employed to fabricate various fluorescent metal nanostructures [277–280]. Particularly, DNA oligonucleotides are excellent stabilizers for preparing small Ag NCs, due to the high affinity between silver ions and cytosine bases on single-stranded DNA.

Fluorescence imaging relies heavily on stable, biocompatible, highly specific, and sensitive markers. Conventional fluorophores such as organic dyes and fluorescent proteins with limited photostability greatly limit the long-term monitoring tests in vivo, and QDs also showed potential safety concerns for in vivo applications. In contrast, fluorescent metal NCs exhibited bright emission as well as good biocompatibility, making them attractive alternatives as fluorescent probes for bioimaging. For instance, ultrasmall bovine serum albumin-stabilized Au NCs exhibiting bright NIR fluorescence and high photostability were successfully used for in vivo

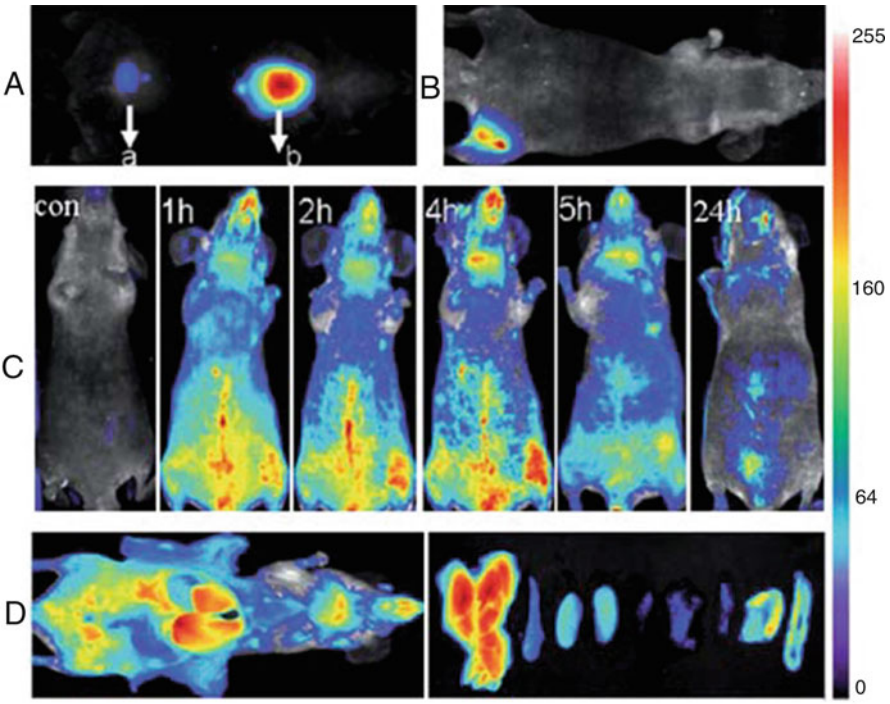

Fig. 2.25 In vivo tumor imaging upon (**a**) subcutaneous (*a*, 0.235 mg mL^{-1}; *b*, 2.35 mg mL^{-1}) and (**b**) intramuscular (2.35 mg mL^{-1}) injection of 100 μL Au NCs into mice. (**c**) Real-time in vivo fluorescence image of abdomen after intravenous injection with Au NCs (200 μL, 2.35 mg mL^{-1}) at different time. (**d**) Ex vivo optical images of a mouse treated with the injection of Au NCs (200 μL, 2.35 mg mL^{-1}) and some dissected organs [276] (Reprinted with permission from Ref. [276], Copyright 2010 the Royal Society of Chemistry)

fluorescence imaging of tumor [276]. Due to the high photostability and low toxicity, the Au NCs could be employed for continuous in vivo imaging. For example, fluorescent Au NCs were injected intravenously into mice for whole-body real-time in vivo imaging. As shown in Fig. 2.25, Au NCs showed spectrally distinguished emission with different brightness depending on locations and the dose of Au NCs injected. The fluorescence of Au NCs could also be visualized upon the injection into muscles by up to a few millimeters on account of their NIR light excitation. The fluorescence of superficial vasculature of mouse was immediately visualized after tail vein injection, remained visible after 5 h, and decreased noticeably after 24 h. Due to the EPR effect, ultrasmall Au NCs were found to accumulate at a high concentration in the tumor sites under in vivo imaging test.

It is important to develop contrast agents with efficient renal clearance for in vivo bioimaging applications. Ideal nanoparticle-based fluorescent probes should be effectively excreted out of the body, with low accumulation in normal organs and minor interference from background noise. Although NCs with hydrodynamic

diameters smaller than 10 nm are usually considered to be stealthy to the reticulo-endothelial system (RES), fluorescent NCs are still severely hampered by their slow renal clearance. To overcome the problem, 2 nm glutathione-coated luminescent Au NCs with good renal clearance were developed. In this case, less than 5% particles were accumulated in the liver, and more than 50% particles were found in urine within 24 h after intravenous injection [281]. Due to the ultrasmall size of fluorescent nanoparticles and biocompatible glutathione ligand, most of Au NCs can keep stable during blood circulation and efficiently be cleared out of the body via the kidney filtration.

In vivo fluorescence imaging of tumors is one of the most important topics in nanomedicine and biomedical engineering for early, accurate tumor diagnosis and imaging-guided surgery and therapy. Due to the facile function of engineered NCs, multimodal imaging-guided combinational phototherapy by integrating various building blocks would be used for cancer diagnosis and therapy. For example, nano-assembly of nanorods (NR) and UCNPs engineered by DNA hybridization was successfully employed for multimodal imaging and combinational phototherapy (Fig. 2.26) [282]. Upon the execution into mice, the assembly exhibited outstanding cancer-targeting ability via EPR effect and substantially eliminated the tumor for in vivo cancer therapy.

5.2.9 Fluorescent Silica Nanoparticles

Since silica nanoparticles (SiNPs) feature optical transparency, robustness, chemical and mechanical stability, low toxicity, easy excrement, and resistance to microbial attacks, they are also suitable for bioimaging [21, 56, 283–287]. However, as SiNPs are optically silent in visible and NIR region, improving their bioimaging capability is focused on doping them with other fluorescent materials to form silica-based hybrid nanomaterials. Fortunately, due to the facile modification on the surface, SiNPs are easily functionalized by lots of existing NIR fluorescent materials such as metal-organic and metallic fluorophores [288], organic dyes [22, 289–291], protein [126], UCNPs [292], and QDs [51]. Thus, different fluorescent SiNPs can be obtained by using different kinds of fluorophores.

Most fluorescent SiNPs consist of silica coating on outside of fluorophores, because silica coating enables excellent properties and enhanced performance, such as high stability over a wide range of solution pH, nontoxicity, non-swelling, and efficient light transmission. Furthermore, silica coating offers a variety of targeting ligands by covalent binding, including antibodies, peptides, sugars, and nucleotides.

Doping SiNPs with NIR fluorescent dyes is a simple and convenient approach to prepare NIR fluorescent nanoparticle probes for in vivo imaging. Recently, SiNPs were successfully used for in vivo biomedical applications. For example, 20–25 nm-sized NIR dye-doped silica nanoparticles (ORMOSIL) were synthesized by a normal micellar route and subsequently radiolabeled with iodine-124. The biodistribution of ORMOSIL determined by NIR fluorescence and radiolabeling studies in vivo displayed a major accumulation in RES in mice. Nearly all of the nanoparticles were cleared out of the body through the hepatobiliary excretion, without any sign of organ toxicity [293]. In

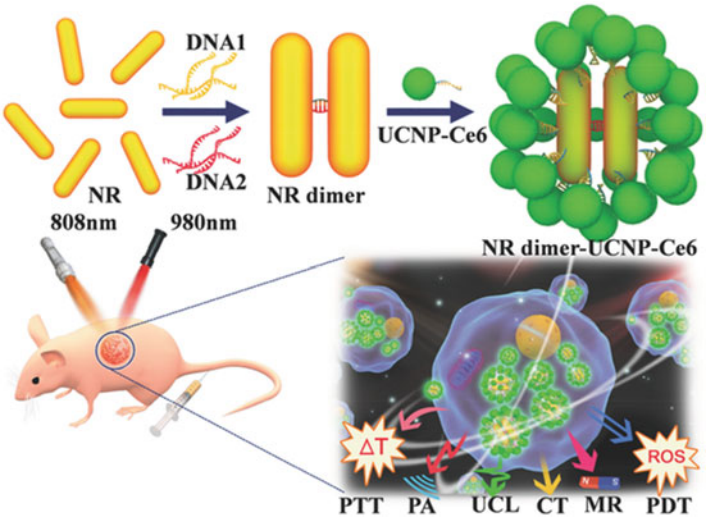

Fig. 2.26 Schematic layout of DNA-hybridized core-satellite assembly of NR dimer and UCNPs for multimodal imaging-guided combinational phototherapy [282] (Reprinted with permission from Ref. [282], Copyright 2016 Wiley-VCH Verlag GmbH & Co. KGaA, Weinheim)

addition, cyanine dye is a type of NIR dye with excellent NIR emission, but with poor photostability strongly limiting its in vivo imaging applications. A promising approach to overcome the problem is incorporating cyanines into SiNPs, where the nanoparticle shell can effectively protect the fluorophore molecules. In a similar case, a unique fluorescent system (CyN-12@NHs) constructed by amphiphilic block copolymer-based nanoscale micelles (NHs) encapsulating NIR fluorescent dye (CyN-12) exhibited good photo and chemical stability, water solubility, and bright NIR fluorescence, making it a suitable fluorescent probe for bioimaging. CyN-12@NHs also showed bright fluorescence with a long retention in tumor by injecting intratumorally into mice and displayed selective accumulation in the liver via intravenous injection [294].

Although fluorescent proteins might be the safest fluorescent probes for in vivo imaging, their instability in the purified forms strongly impeded their uses. Fortunately, near-infrared fluorescent proteins (NIRFPs) coated with a silica nanoshell, named NIRFP@silica, can increase the stability of proteins and simultaneously improve the quantum yield and photostability of the coated NIRFPs. When injected by the tail vein, NIRFP@silica with a small nanoparticle size, narrow distribution, and good dispersibility can be distributed all over the mouse body, and then efficiently eliminated through urine in 24 h, indicating its high potential as a safe and robust NIR fluorescence imaging agent for whole-body imaging. To avoid the adverse interference of pulmonary damage resulted from the aggregation/agglomeration of nanoparticles, nanoprobes with slightly bigger size than a single fluorescent protein were produced via lysine-catalyzed Stöber method [126].

A multifunctional core/satellite nanotheranostic (CSNT) constructed by decorating ultrasmall CuS nanoparticles onto the surface of a silica-coated UCNP could not

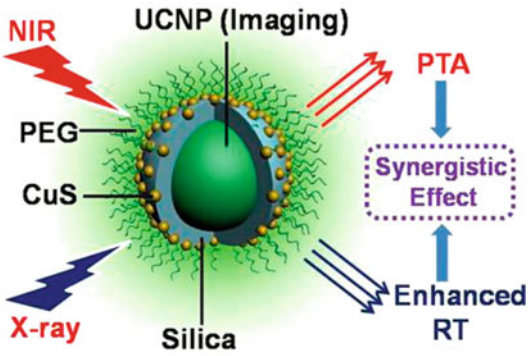

Fig. 2.27 Schematic layout of a synergistic therapy based on CSNT for enhanced radiotherapy (RT) and photothermal ablation (PTA). UCNP cores are responsible for the RT, and CuS satellites are used to convert the 980 nm laser into heat for PTA [292] (Reprinted from Ref. [292], Copyright 2013 the American Chemical Society)

only convert NIR light into heat for effective thermal ablation but also cause highly localized radiation dose boost to trigger remarkably enhanced radiation damage in vivo. Moreover, the CSNT can be used as an excellent trimodal imaging agent based on upconversion luminescence, magnetic resonance, and computer tomography technology (Fig. 2.27) [292]. Similarly, mesoporous SiO_2 can be modified by UCNPs. For example, a microcarrier (Fig. 2.28) based on mesoporous SiO_2-Nd@SiO_2@mSiO_2-NH_2@SSPI (SSPI, succinylated soy protein isolate polymer) was successfully used to noninvasively monitor the gastrointestinal drug release in vivo through the NIR-II fluorescence signals of lanthanide-based downconversion nanoparticles (DCNPs) [295].

In another example, chlorin e6 (Ce_6) photosensitizer conjugated with silica-coated gold nanoclusters (AuNC@SiO_2-Ce_6) can be used for NIR fluorescence imaging of gastric cancer tissue through intravenous injection into MDA-MB-435 breast cancer-bearing mice [296]. Moreover, the persistent emission (5–13 ms) of NIR luminescent nanoparticles made of porous silicon is long enough to permit time-resolved fluorescence imaging and can be distinguished in the time domain from signals associated with tissue autofluorescence or interfering organic chromophores [285].

Compared with other semiconductor nanocrystals, silicon quantum dots (Si QDs) possess many merits including high natural abundance of silicon, low cytotoxicity, unique size, and surface-dependent optical properties [297]. Strategies for the preparation of Si QDs generally include solution-phase-based methods, microemulsion synthesis, and thermally induced disproportionation of solid hydrogen silsesquioxane in a reducing atmosphere. The approaches for the functionalization of Si QDs include surface oxidation and etching, covalent functionalization, non-covalent functionalization, and bioconjugation [34]. Si QDs can be used in multiple cancer-related in vivo imaging, such as tumor vasculature targeting, sentinel lymph node mapping, and multicolor NIR imaging. For example, a type of Si QDs was developed through a combination of unique nanoparticle synthesis, surface functionalization, PEGylated micelle encapsulation, and bioconjugation. The encapsulated Si QDs with nanospheres showed stable luminescence and long tumor accumulation time (>40 h) in live mice [298].

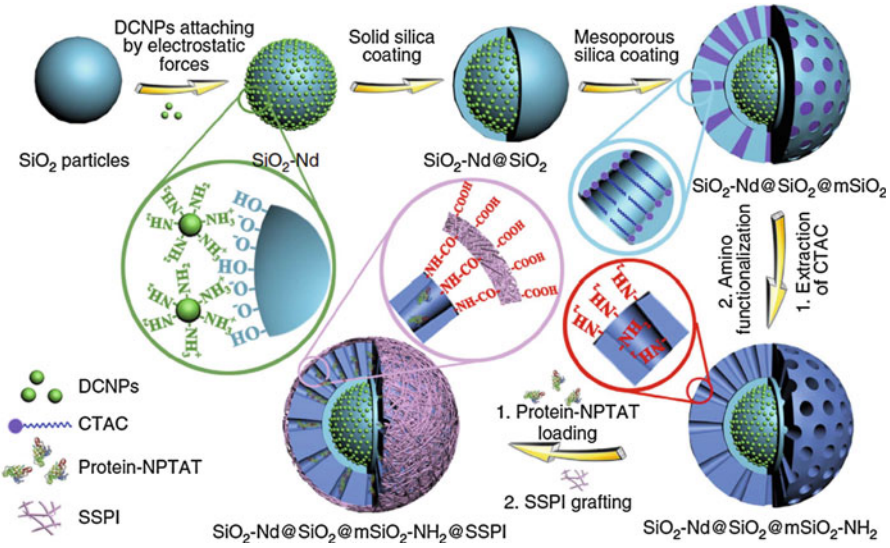

Fig. 2.28 Schematic illustration of NIR-II fluorescent mesoporous microcarrier preparation with protein drugs loading and SSPI grafting. NPTAT, nickel(II) phthalocyanine-tetrasulfonic acid tetrasodium; CTAC, cetyltrimethylammonium chloride [295] (Reprinted from Ref. [295], Copyright 2017 Nature Publishing Group)

6 Conclusions and Future Perspective

NIR fluorescence is a powerful imaging technique that not only noninvasively visualizes biological processes in cells and organisms but also permits tracking of molecules and cells in real time for disease diagnosis and treatment. Thus, ideal NIR fluorescent materials with strong luminescence, desirable excitation and emission wavelength, high photostability, small size, and good biocompatibility are pivotal for in vivo imaging. However, the lack of desirable NIR fluorescent probes is the major reason that NIR fluorescence imaging in vivo is still in its infancy of clinical diagnosis and therapy. Moreover, some problems still limit clinical applications of NIR fluorescence imaging, such as the degradation of imaging agents, the toxicity to bio-samples, and color fading.

NIR fluorescent materials with excellent photophysical properties and smart functionality are not only basic elements of theranostic techniques for biology and pathophysiology but also practically significant toward clinical applications. For optimal monitoring and deciphering of physiological structures and functions with the maximum temporal and spatial resolution as well as minimal perturbation to biological systems, NIR fluorescent probes should have high brightness, adequate water dispersibility, excellent biocompatibility, and facile bioconjugation. Among many NIR fluorescent materials, small fluorophores (such as NIR dyes and metal complexes) and fluorescent proteins have been extensively studied for bioimaging

in vivo. However, these small fluorophores and fluorescent proteins generally show photo-bleaching that limits their maximum effectiveness for long-range and three-dimensional in vivo imaging. Despite great advances that have been made in the field of NIR dyes for bioimaging, there are still a lot of rooms for further improvement. For instance, some cyanine dyes still suffer from low photostability, which should be further improved. The ease of aggregation in aqueous media greatly limits squaraines for medical and biological imaging. To improve the photostability of cyanine dyes and reduce their cell toxicity, tremendous efforts have been given to cyanine-based contrast agents. Rational incorporation of the cyanine platform with nanoparticles or polymers has provided great opportunities to efficiently monitor the biological species in tissue and animal body. The approaches for the conjugation of nanoparticles such as UCNPs or QDs could be built up to enhance the performance of NIR dyes for bioimaging.

Nanoparticles like QDs have been frequently employed for bioimaging applications. However, these QDs usually contain inherently toxic elements including cadmium and selenium that are easy to leak and harm to live organisms, which severely restrict their uses to most in vivo work and narrow their scope of applications. Furthermore, QDs with dynamic surface structures tend to aggregate in biological environments, which also constrain their physiological utilities and clinical implementation. To overcome these limitations, silicon nanocrystals, C-dots, and GQDs featuring higher photostability and better biocompatibility have been developed. On the other hand, it is not easy to tune broad photoluminescence emission for GQDs and to gain pure samples of CNTs with desirable photoluminescence intensity. Although silicon nanocrystals and C-dots have demonstrated increasing importance in the field of biological imaging, some questions regarding the complete understanding of their fluorescence mechanism and rational control of their emission characteristics still remain. Unlike these materials, the photoluminescence of nanodiamond is known to rely mainly on the formation of well-established fluorescent NV centers. However, nanodiamond possesses low extinction coefficient and their emission is not easily tunable.

As discussed in this chapter, numerous NIR fluorescent probes, including organic dyes, fluorescent proteins, and nanoparticles, have been used for fluorescence bioimaging. Most of them for bioimaging take advantage of single-photon excitation, emitting long wavelength fluorescence when excited by low wavelength light. In contrast, by using the anti-Stokes luminescence process, two-photon-excited fluorescence imaging offers a powerful approach for bioimaging of the living tissue to eliminate autofluorescence. Due to the requirement of simultaneous absorption of two coherent photons, these two-photon fluorescence materials usually exhibit narrow two-photon absorption cross sections and low two-photon emission efficiency. In addition, expensive pulsed lasers (usually a femtosecond laser) are needed for two-photon fluorescence imaging.

On account of intrinsic upconversion luminescent features and narrow emission lines, UCNPs have attracted significant attention, providing lots of uncommon opportunities in bioimaging applications. On the other hand, their drawbacks include less facile bioconjugation and larger size. The safety concern of UCNPs in

biomedical application cannot be ignored. Thus, how to design and develop safer and smarter UCNPs with enhanced quantum yields is a right research direction in this rapidly developing field. For nanosystems based on SiNPs, they have very bright fluorescence and possess excellent resistance to photo-bleaching. But, less facile multiplexing and large size hamper their practical use. Thus, it is necessary to design optimal and functional structures to enhance their biomedical performance by chemical modifications and bioconjugation, and detailed in vivo biosafety and performance investigations are also required. Furthermore, the synergistic combination of inorganic SiO_2 and organic functionalities is expected to highly facilitate the clinical translation of these nanosystems. In short, each type of fluorescent materials possesses their own merits and shortages. Choosing a right system for NIR fluorescent bioimaging depends on their performance for a specific biological task.

Acknowledgment This work was financially supported by the SingHealth-NTU Research Collaborative Grant (SHS-NTU/009/2016) and the Singapore Academic Research Fund (RG121/16 (S)).

References

1. Erathodiyil N, Ying JY (2011) Functionalization of inorganic nanoparticles for bioimaging applications. Acc Chem Res 44:925–935
2. Ueno T, Nagano T (2011) Fluorescent probes for sensing and imaging. Nat Method 8:642–645
3. Kobayashi H, Ogawa M, Alford R, Choyke PL et al (2010) New strategies for fluorescent probe design in medical diagnostic imaging. Chem Rev 110:2620–2640
4. Chengzhou Z, Dan D, Yuehe L (2015) Graphene and graphene-like 2D materials for optical biosensing and bioimaging: a review. 2D Mater 2:032004
5. Bardhan R, Lal S, Joshi A, Halas NJ (2011) Theranostic nanoshells: from probe design to imaging and treatment of cancer. Acc Chem Res 44:936–946
6. Ding C, Zhu A, Tian Y (2014) Functional surface engineering of C-dots for fluorescent biosensing and in vivo bioimaging. Acc Chem Res 47:20–30
7. Hsiao WW-W, Hui YY, Tsai P-C, Chang H-C (2016) Fluorescent nanodiamond: a versatile tool for long-term cell tracking, super-resolution imaging, and nanoscale temperature sensing. Acc Chem Res 49:400–407
8. Owens EA, Henary M, El Fakhri G, Choi HS (2016) Tissue-specific near-infrared fluorescence imaging. Acc Chem Res 49:1731–1740
9. Yuan L, Lin W, Zheng K, Zhu S (2013) FRET-based small-molecule fluorescent probes: rational design and bioimaging applications. Acc Chem Res 46:1462–1473
10. Zhu H, Fan J, Du J, Peng X (2016) Fluorescent probes for sensing and imaging within specific cellular organelles. Acc Chem Res 49:2115–2126
11. Lin J, Chen X, Huang P (2016) Graphene-based nanomaterials for bioimaging. Adv Drug Deliv Rev 105, Part B:242–254
12. Pu K-Y, Liu B (2011) Fluorescent conjugated polyelectrolytes for bioimaging. Adv Funct Mater 21:3408–3423
13. Xing P, Zhao Y (2016) Multifunctional nanoparticles self-assembled from small organic building blocks for biomedicine. Adv Mater 28:7304–7339
14. Tan G-R, Wang M, Hsu C-Y, Chen N et al (2016) Small upconverting fluorescent nanoparticles for biosensing and bioimaging. Adv Opt Mater 4:984–997
15. Kushida Y, Nagano T, Hanaoka K (2015) Silicon-substituted xanthene dyes and their applications in bioimaging. Analyst 140:685–695

16. Li J, Zhu J-J (2013) Quantum dots for fluorescent biosensing and bio-imaging applications. Analyst 138:2506–2515
17. Hahn MA, Singh AK, Sharma P, Brown SC et al (2011) Nanoparticles as contrast agents for in-vivo bioimaging: current status and future perspectives. Anal Bioanal Chem 399:3–27
18. Umezawa K, Citterio D, Suzuki K (2014) New trends in near-infrared fluorophores for bioimaging. Anal Sci 30:327–349
19. Chakraborty K, Veetil AT, Jaffrey SR, Krishnan Y (2016) Nucleic acid–based nanodevices in biological imaging. Annu Rev Biochem 85:349–373
20. Petryayeva E, Algar WR, Medintz IL (2013) Quantum dots in bioanalysis: a review of applications across various platforms for fluorescence spectroscopy and imaging. Appl Spectrosc 67:215–252
21. Du X, Li X, Xiong L, Zhang X et al (2016) Mesoporous silica nanoparticles with organo-bridged silsesquioxane framework as innovative platforms for bioimaging and therapeutic agent delivery. Biomaterials 91:90–127
22. Bae SW, Tan W, Hong J-I (2012) Fluorescent dye-doped silica nanoparticles: new tools for bioapplications. Chem Commun 48:2270–2282
23. Georgakilas V, Tiwari JN, Kemp KC, Perman JA et al (2016) Noncovalent functionalization of graphene and graphene oxide for energy materials, biosensing, catalytic, and biomedical applications. Chem Rev 116:5464–5519
24. Louie A (2010) Multimodality imaging probes: design and challenges. Chem Rev 110:3146–3195
25. Smith BR, Gambhir SS (2017) Nanomaterials for in vivo imaging. Chem Rev 117:901–986
26. Sun W, Guo S, Hu C, Fan J et al (2016) Recent development of chemosensors based on cyanine platforms. Chem Rev 116:7768–7817
27. Yang Y, Zhao Q, Feng W, Li F (2013) Luminescent chemodosimeters for bioimaging. Chem Rev 113:192–270
28. Yao J, Yang M, Duan Y (2014) Chemistry, biology, and medicine of fluorescent nanomaterials and related systems: new insights into biosensing, bioimaging, genomics, diagnostics, and therapy. Chem Rev 114:6130–6178
29. Wang L-J, Ma F, Tang B, Zhang C-Y (2017) Sensing telomerase: from in vitro detection to in vivo imaging. Chem Sci 8:2495–2502
30. Amoroso AJ, Pope SJA (2015) Using lanthanide ions in molecular bioimaging. Chem Soc Rev 44:4723–4742
31. Ashton TD, Jolliffe KA, Pfeffer FM (2015) Luminescent probes for the bioimaging of small anionic species in vitro and in vivo. Chem Soc Rev 44:4547–4595
32. Chen X, Zhang W (2017) Diamond nanostructures for drug delivery, bioimaging, and biosensing. Chem Soc Rev 46:734–760
33. Meng H-M, Liu H, Kuai H, Peng R et al (2016) Aptamer-integrated DNA nanostructures for biosensing, bioimaging and cancer therapy. Chem Soc Rev 45:2583–2602
34. Montalti M, Cantelli A, Battistelli G (2015) Nanodiamonds and silicon quantum dots: ultrastable and biocompatible luminescent nanoprobes for long-term bioimaging. Chem Soc Rev 44:4853–4921
35. Tang Y, Lee D, Wang J, Li G et al (2015) Development of fluorescent probes based on protection-deprotection of the key functional groups for biological imaging. Chem Soc Rev 44:5003–5015
36. Wegner KD, Hildebrandt N (2015) Quantum dots: bright and versatile in vitro and in vivo fluorescence imaging biosensors. Chem Soc Rev 44:4792–4834
37. Wolfbeis OS (2015) An overview of nanoparticles commonly used in fluorescent bioimaging. Chem Soc Rev 44:4743–4768
38. Wu P, Yan X-P (2013) Doped quantum dots for chemo/biosensing and bioimaging. Chem Soc Rev 42:5489–5521
39. Wu X, Zhu W (2015) Stability enhancement of fluorophores for lighting up practical application in bioimaging. Chem Soc Rev 44:4179–4184

40. Yang Z, Cao J, He Y, Yang JH et al (2014) Macro−/micro-environment-sensitive chemosensing and biological imaging. Chem Soc Rev 43:4563–4601
41. Yang Z, Sharma A, Qi J, Peng X et al (2016) Super-resolution fluorescent materials: an insight into design and bioimaging applications. Chem Soc Rev 45:4651–4667
42. Yoo JM, Kang JH, Hong BH (2015) Graphene-based nanomaterials for versatile imaging studies. Chem Soc Rev 44:4835–4852
43. Zhao Q, Huang C, Li F (2011) Phosphorescent heavy-metal complexes for bioimaging. Chem Soc Rev 40:2508–2524
44. Zhou J, Liu Z, Li F (2012) Upconversion nanophosphors for small-animal imaging. Chem Soc Rev 41:1323–1349
45. Zrazhevskiy P, Sena M, Gao X (2010) Designing multifunctional quantum dots for bioimaging, detection, and drug delivery. Chem Soc Rev 39:4326–4354
46. LeCroy GE, Yang S-T, Yang F, Liu Y et al (2016) Functionalized carbon nanoparticles: syntheses and applications in optical bioimaging and energy conversion. Coord Chem Rev 320–321:66–81
47. Liu Q, Feng W, Li F (2014) Water-soluble lanthanide upconversion nanophosphors: synthesis and bioimaging applications in vivo. Coord Chem Rev 273–274:100–110
48. Mukherjee A, Schroeder CM (2015) Flavin-based fluorescent proteins: emerging paradigms in biological imaging. Curr Opin Biotechnol 31:16–23
49. Escobedo JO, Rusin O, Lim S, Strongin RM (2010) NIR dyes for bioimaging applications. Curr Opin Chem Biol 14:64
50. Becker JS (2010) Bioimaging of metals in brain tissue from micrometre to nanometre scale by laser ablation inductively coupled plasma mass spectrometry: state of the art and perspectives. Int J Mass Spectrom 289:65–75
51. Gomes MC, Cunha Â, Trindade T, Tomé JPC (2016) The role of surface functionalization of silica nanoparticles for bioimaging. J Innov Opt Health Sci 09:1630005
52. Chen S, Wang H, Hong Y, Tang BZ (2016) Fabrication of fluorescent nanoparticles based on AIE luminogens (AIE dots) and their applications in bioimaging. Mater Horiz 3:283–293
53. Du D, Yang Y, Lin Y (2012) Graphene-based materials for biosensing and bioimaging. MRS Bull 37:1290–1296
54. Hemmer E, Venkatachalam N, Hyodo H, Hattori A et al (2013) Upconverting and NIR emitting rare earth based nanostructures for NIR-bioimaging. Nanoscale 5:11339–11361
55. Chudakov DM, Matz MV, Lukyanov S, Lukyanov KA (2010) Fluorescent proteins and their applications in imaging living cells and tissues. Physiol Rev 90:1103–1163
56. Niu J, Wang X, Lv J, Li Y et al (2014) Luminescent nanoprobes for in-vivo bioimaging. TrAC Trends Anal Chem 58:112–119
57. Yu M, Li F, Chen Z, Hu H et al (2009) Laser scanning up-conversion luminescence microscopy for imaging cells labeled with rare-earth nanophosphors. Anal Chem 81:930–935
58. So PTC, Dong CY, Masters BR, Berland KM (2000) Two-photon excitation fluorescence microscopy. Annu Rev Biomed Eng 2:399–429
59. Yi M, Yang S, Peng Z, Liu C et al (2014) Two-photon graphene oxide/aptamer nanosensing conjugate for in vitro or in vivo molecular probing. Anal Chem 86:3548–3554
60. Nagano T (2010) Development of fluorescent probes for bioimaging applications. Proc Jpn Acad Ser B 86:837–847
61. Chan J, Dodani SC, Chang CJ (2012) Reaction-based small-molecule fluorescent probes for chemoselective bioimaging. Nat Chem 4:973–984
62. Barbieri A, Bandini E, Monti F, Praveen VK et al (2016) The rise of near-infrared emitters: organic dyes, porphyrinoids, and transition metal complexes. Top Curr Chem 374:47
63. Yuan L, Lin W, Zheng K, He L et al (2013) Far-red to near infrared analyte-responsive fluorescent probes based on organic fluorophore platforms for fluorescence imaging. Chem Soc Rev 42:622–661
64. Isago H (2015) Optical spectra of phthalocyanines and related compounds: a guide for beginners. Springer, Tokyo, pp 107–132
65. Owens EA, Hyun H, Kim SH, Lee JH et al (2013) Highly charged cyanine fluorophores for trafficking scaffold degradation. Biomed Mater 8:014109

66. Park JH, Royer JE, Chagarov E, Kaufman-Osborn T et al (2013) Atomic imaging of the irreversible sensing mechanism of NO_2 adsorption on copper phthalocyanine. J Am Chem Soc 135:14600–14609
67. Chen X, Pradhan T, Wang F, Kim JS et al (2012) Fluorescent chemosensors based on spiroring-opening of xanthenes and related derivatives. Chem Rev 112:1910–1956
68. Katori A, Azuma E, Ishimura H, Kuramochi K et al (2015) Fluorescent dyes with directly connected xanthone and xanthene units. J Org Chem 80:4603–4610
69. He X, Wu X, Wang K, Shi B et al (2009) Methylene blue-encapsulated phosphonate-terminated silica nanoparticles for simultaneous in vivo imaging and photodynamic therapy. Biomaterials 30:5601–5609
70. Oushiki D, Kojima H, Terai T, Arita M et al (2010) Development and application of a near-infrared fluorescence probe for oxidative stress based on differential reactivity of linked cyanine dyes. J Am Chem Soc 132:2795–2801
71. Peng X, Song F, Lu E, Wang Y et al (2005) Heptamethine cyanine dyes with a large stokes shift and strong fluorescence: a paradigm for excited-state intramolecular charge transfer. J Am Chem Soc 127:4170–4171
72. Tasior M, O'Shea DF (2010) BF2-chelated tetraarylazadipyrromethenes as NIR fluorochromes. Bioconjug Chem 21:1130–1133
73. Pansare VJ, Hejazi S, Faenza WJ, Prud'homme RK (2012) Review of long-wavelength optical and NIR imaging materials: contrast agents, fluorophores, and multifunctional nano carriers. Chem Mater 24:812–827
74. Choi HS, Nasr K, Alyabyev S, Feith D et al (2011) Synthesis and in vivo fate of zwitterionic near-infrared fluorophores. Angew Chem Int Ed 50:6258–6263
75. Rong P, Huang P, Liu Z, Lin J et al (2015) Protein-based photothermal theranostics for imaging-guided cancer therapy. Nanoscale 7:16330–16336
76. Owens EA, Hyun H, Tawney JG, Choi HS et al (2015) Correlating molecular character of NIR imaging agents with tissue-specific uptake. J Med Chem 58:4348–4356
77. Zhang K, Zhang J, Xi Z, Li L-Y et al (2017) A new H_2S-specific near-infrared fluorescence-enhanced probe that can visualize the H_2S level in colorectal cancer cells in mice. Chem Sci 8:2776–2781
78. Hyun H, Wada H, Bao K, Gravier J et al (2014) Phosphonated near-infrared fluorophores for biomedical imaging of bone. Angew Chem Int Ed 53:10668–10672
79. Hyun H, Owens EA, Wada H, Levitz A et al (2015) Cartilage-specific near-infrared fluorophores for biomedical imaging. Angew Chem Int Ed 54:8648–8652
80. Choi HS, Gibbs SL, Lee JH, Kim SH et al (2013) Targeted zwitterionic near-infrared fluorophores for improved optical imaging. Nat Biotechnol 31:148–153
81. Hyun H, Park MH, Owens EA, Wada H et al (2015) Structure-inherent targeting of near-infrared fluorophores for parathyroid and thyroid gland imaging. Nat Med 21:192–197
82. Fischer GM, Jungst C, Isomaki-Krondahl M, Gauss D et al (2010) Asymmetric PPCys: strongly fluorescing NIR labels. Chem Commun 46:5289–5291
83. Anees P, Joseph J, Sreejith S, Menon NV et al (2016) Real time monitoring of aminothiol level in blood using a near-infrared dye assisted deep tissue fluorescence and photoacoustic bimodal imaging. Chem Sci 7:4110–4116
84. Avirah RR, Jayaram DT, Adarsh N, Ramaiah D (2012) Squaraine dyes in PDT: from basic design to in vivo demonstration. Org Biomol Chem 10:911–920
85. Hu L, Yan Z, Xu H (2013) Advances in synthesis and application of near-infrared absorbing squaraine dyes. RSC Adv 3:7667–7676
86. Beverina L, Salice P (2010) Squaraine compounds: tailored design and synthesis towards a variety of material science applications. Eur J Org Chem 2010:1207–1225
87. Anees P, Sreejith S, Ajayaghosh A (2014) Self-assembled near-infrared dye nanoparticles as a selective protein sensor by activation of a dormant fluorophore. J Am Chem Soc 136:13233–13239
88. Baumes JM, Gassensmith JJ, Giblin J, Lee J-J et al (2010) Storable, thermally activated, near-infrared chemiluminescent dyes and dye-stained microparticles for optical imaging. Nat Chem 2:1025–1030

89. A. Poirel, A. De Nicola and R. Ziessel, Oligothienyl-BODIPYs: red and near-infrared emitters, Org Lett, 2012, 14: 5696–5699
90. Ni Y, Wu J (2014) Far-red and near infrared BODIPY dyes: synthesis and applications for fluorescent pH probes and bio-imaging. Org Biomol Chem 12:3774–3791
91. Zhang X, Yu H, Xiao Y (2012) Replacing phenyl ring with thiophene: an approach to longer wavelength aza-dipyrromethene boron difluoride (Aza-BODIPY) dyes. J Org Chem 77:669–673
92. Lu H, Mack J, Yang Y, Shen Z (2014) Structural modification strategies for the rational design of red/NIR region BODIPYs. Chem Soc Rev 43:4778–4823
93. Loudet A, Burgess K (2007) BODIPY dyes and their derivatives: syntheses and spectroscopic properties. Chem Rev 107:4891–4932
94. Ulrich G, Ziessel R, Harriman A (2008) The chemistry of fluorescent bodipy dyes: versatility unsurpassed. Angew Chem Int Ed 47:1184–1201
95. Tasior M, Murtagh J, Frimannsson DO, McDonnell SO et al (2010) Water-solubilised BF2-chelated tetraarylazadipyrromethenes. Org Biomol Chem 8:522–525
96. Jiang N, Fan J, Liu T, Cao J et al (2013) A near-infrared dye based on BODIPY for tracking morphology changes in mitochondria. Chem Commun 49:10620–10622
97. Wu H, Krishnakumar S, Yu J, Liang D et al (2014) Highly selective and sensitive near-infrared-fluorescent probes for the detection of cellular hydrogen sulfide and the imaging of H_2S in mice. Chem Asian J 9:3604–3611
98. Tian J, Zhou J, Shen Z, Ding L et al (2015) A pH-activatable and aniline-substituted photosensitizer for near-infrared cancer theranostics. Chem Sci 6:5969–5977
99. McQuade LE, Ma J, Lowe G, Ghatpande A et al (2010) Visualization of nitric oxide production in the mouse main olfactory bulb by a cell-trappable copper(II) fluorescent probe. Proc Natl Acad Sci 107:8525–8530
100. Koide Y, Urano Y, Hanaoka K, Piao W et al (2012) Development of NIR fluorescent dyes based on Si–rhodamine for in vivo imaging. J Am Chem Soc 134:5029–5031
101. Yuan L, Lin W, Yang Y, Chen H (2012) A unique class of near-infrared functional fluorescent dyes with carboxylic-acid-modulated fluorescence ON/OFF switching: rational design, synthesis, optical properties, theoretical calculations, and applications for fluorescence imaging in living animals. J Am Chem Soc 134:1200–1211
102. Koide Y, Urano Y, Hanaoka K, Terai T et al (2011) Development of an Si-rhodamine-based far-red to near-infrared fluorescence probe selective for hypochlorous acid and its applications for biological imaging. J Am Chem Soc 133:5680–5682
103. Bhupathiraju NVSDK, Rizvi W, Batteas JD, Drain CM (2016) Fluorinated porphyrinoids as efficient platforms for new photonic materials, sensors, and therapeutics. Org Biomol Chem 14:389–408
104. Babu SS, Bonifazi D (2014) Self-organization of polar porphyrinoids. ChemPlusChem 79:895–906
105. Sommer JR, Shelton AH, Parthasarathy A, Ghiviriga I et al (2011) Photophysical properties of near-infrared phosphorescent π-extended platinum porphyrins. Chem Mater 23:5296–5304
106. Lovell JF, Jin CS, Huynh E, Jin H et al (2011) Porphysome nanovesicles generated by porphyrin bilayers for use as multimodal biophotonic contrast agents. Nat Mater 10:324–332
107. Kim J, Tung C-H, Choi Y (2014) Smart dual-functional warhead for folate receptor-specific activatable imaging and photodynamic therapy. Chem Commun 50:10600–10603
108. Lee H, Kim J, Kim H, Kim Y et al (2014) A folate receptor-specific activatable probe for near-infrared fluorescence imaging of ovarian cancer. Chem Commun 50:7507–7510
109. Yang Q, Ma Z, Wang H, Zhou B et al (2017) Rational design of molecular fluorophores for biological imaging in the NIR-II window. Adv Mater 29:1605497
110. Divya KP, Sreejith S, Ashokkumar P, Yuzhan K et al (2014) A ratiometric fluorescent molecular probe with enhanced two-photon response upon Zn2+ binding for in vitro and in vivo bioimaging. Chem Sci 5:3469–3474

111. Tian J, Ding L, Xu H-J, Shen Z et al (2013) Cell-specific and pH-activatable rubyrin-loaded nanoparticles for highly selective near-infrared photodynamic therapy against cancer. J Am Chem Soc 135:18850–18858
112. Sun W, Fan J, Hu C, Cao J et al (2013) A two-photon fluorescent probe with near-infrared emission for hydrogen sulfide imaging in biosystems. Chem Commun 49:3890–3892
113. Chen Y, Guan R, Zhang C, Huang J et al (2016) Two-photon luminescent metal complexes for bioimaging and cancer phototherapy. Coord Chem Rev 310:16–40
114. Zhang KY, Liu S, Zhao Q, Li F et al (2015) In: Lo KK-W (ed) Luminescent and photoactive transition metal complexes as biomolecular probes and cellular reagents. Springer, Berlin/Heidelberg, pp 131–180
115. Jing J, Chen J-J, Hai Y, Zhan J et al (2012) Rational design of ZnSalen as a single and two photon activatable fluorophore in living cells. Chem Sci 3:3315–3320
116. Xie D, Jing J, Cai Y-B, Tang J et al (2014) Construction of an orthogonal ZnSalen/Salophen library as a colour palette for one- and two-photon live cell imaging. Chem Sci 5:2318–2327
117. Shu X, Royant A, Lin MZ, Aguilera TA et al (2009) Mammalian expression of infrared fluorescent proteins engineered from a bacterial phytochrome. Science 324:804–807
118. Allison RR (2016) Fluorescence guided resection (FGR): a primer for oncology. Photodiagn Photodyn Ther 13:73–80
119. Lin MZ (2011) Beyond the rainbow: new fluorescent proteins brighten the infrared scene. Nat Method 8:726–728
120. Lecoq J, Schnitzer MJ (2011) An infrared fluorescent protein for deeper imaging. Nat Biotechnol 29:715–716
121. Shcherbo D, Shemiakina II, Ryabova AV, Luker KE et al (2010) Near-infrared fluorescent proteins. Nat Method 7:827–829
122. Filonov GS, Piatkevich KD, Ting L-M, Zhang J et al (2011) Bright and stable near-infrared fluorescent protein for in vivo imaging. Nat Biotechnol 29:757–761
123. Gong H, Kovar J, Little G, Chen H et al (2010) In vivo imaging of xenograft tumors using an epidermal growth factor receptor-specific affibody molecule labeled with a near-infrared fluorophore. Neoplasia (New York) 12:139–149
124. He J, Wang Y, Missinato MA, Onuoha E et al (2016) A genetically targetable near-infrared photosensitizer. Nat Method 13:263–268
125. Wang Y, Ballou B, Schmidt BF, Andreko S et al (2017) Affibody-targeted fluorogen activating protein for in vivo tumor imaging. Chem Commun 53:2001–2004
126. Yang Y, Xiang K, Yang Y-X, Wang Y-W et al (2013) An individually coated near-infrared fluorescent protein as a safe and robust nanoprobe for in vivo imaging. Nanoscale 5:10345–10352
127. Hong H, Goel S, Zhang Y, Cai W (2011) Molecular imaging with nucleic acid aptamers. Curr Med Chem 18:4195–4205
128. Mallikaratchy PR, Ruggiero A, Gardner JR, Kuryavyi V et al (2011) A multivalent DNA aptamer specific for the B-cell receptor on human lymphoma and leukemia. Nucleic Acids Res 39:2458–2469
129. Shi H, He X, Wang K, Wu X et al (2011) Activatable aptamer probe for contrast-enhanced in vivo cancer imaging based on cell membrane protein-triggered conformation alteration. Proc Natl Acad Sci 108:3900–3905
130. Gong P, Shi B, Zheng M, Wang B et al (2012) PEI protected aptamer molecular probes for contrast-enhanced in vivo cancer imaging. Biomaterials 33:7810–7817
131. Choi HMT, Beck VA, Pierce NA (2014) Next-generation in situ hybridization chain reaction: higher gain, lower cost, greater durability. ACS Nano 8:4284–4294
132. Choi HMT, Chang JY, Trinh LA, Padilla JE et al (2010) Programmable in situ amplification for multiplexed imaging of mRNA expression. Nat Biotechnol 28:1208–1212
133. Hu S-H, Gao X (2010) Nanocomposites with spatially separated functionalities for combined imaging and magnetolytic therapy. J Am Chem Soc 132:7234–7237

134. Zhang X, Wang S, Xu L, Feng L et al (2012) Biocompatible polydopamine fluorescent organic nanoparticles: facile preparation and cell imaging. Nanoscale 4:5581–5584
135. Wang X-d, Meier RJ, Wolfbeis OS (2012) A fluorophore-doped polymer nanomaterial for referenced imaging of pH and temperature with sub-micrometer resolution. Adv Funct Mater 22:4202–4207
136. Schreml S, Meier RJ, Kirschbaum M, Kong SC et al (2014) Luminescent dual sensors reveal extracellular pH-gradients and hypoxia on chronic wounds that disrupt epidermal repair. Theranostics 4:721–735
137. Li Y, Yang HY, Lee DS (2016) Polymer-based and pH-sensitive nanobiosensors for imaging and therapy of acidic pathological areas. Pharm Res 33:2358–2372
138. Tuncel D, Demir HV (2010) Conjugated polymer nanoparticles. Nanoscale 2:484–494
139. Xu H, Wang L, Fan C (2012) Functional nanoparticles for bioanalysis. Nanomedicine, and bioelectronic devices, vol 1. ACS symposium series, vol 1112, Chapter 4. American Chemical Society, Washington, DC, pp 81–117
140. Wu C, Szymanski C, Cain Z, McNeill J (2007) Conjugated polymer dots for multiphoton fluorescence imaging. J Am Chem Soc 129:12904–12905
141. Kim S, Lim C-K, Na J, Lee Y-D et al (2010) Conjugated polymer nanoparticles for biomedical in vivo imaging. Chem Commun 46:1617–1619
142. Li K, Liu Y, Pu K-Y, Feng S-S et al (2011) Polyhedral oligomeric silsesquioxanes-containing conjugated polymer loaded PLGA nanoparticles with trastuzumab (herceptin) functionalization for HER2-positive cancer cell detection. Adv Funct Mater 21:287–294
143. Shuhendler AJ, Pu K, Cui L, Uetrecht JP et al (2014) Real-time imaging of oxidative and nitrosative stress in the liver of live animals for drug-toxicity testing. Nat Biotechnol 32:373–380
144. Klingstedt T, Nilsson KPR (2011) Conjugated polymers for enhanced bioimaging. Biochim Biophys Acta Gen Subj 1810:286–296
145. Jeong K, Park S, Lee Y-D, Lim C-K et al (2013) Conjugated polymer/photochromophore binary nanococktails: bistable photoswitching of near-infrared fluorescence for in vivo imaging. Adv Mater 25:5574–5580
146. Ding D, Liu J, Feng G, Li K et al (2013) Bright far-red/near-infrared conjugated polymer nanoparticles for in vivo bioimaging. Small 9:3093–3102
147. Greenham NC, Moratti SC, Bradley DDC, Friend RH et al (1993) Efficient light-emitting diodes based on polymers with high electron affinities. Nature 365:628–630
148. Lyu Y, Pu K (2017) Recent advances of activatable molecular probes based on semiconducting polymer nanoparticles in sensing and imaging. Adv Sci 4:1600481
149. Zhu H, Fang Y, Zhen X, Wei N et al (2016) Multilayered semiconducting polymer nanoparticles with enhanced NIR fluorescence for molecular imaging in cells, zebrafish and mice. Chem Sci 7:5118–5125
150. Jin Y, Ye F, Zeigler M, Wu C et al (2011) Near-infrared fluorescent dye-doped semiconducting polymer dots. ACS Nano 5:1468–1475
151. Pu K, Shuhendler AJ, Rao J (2013) Semiconducting polymer nanoprobe for in vivo imaging of reactive oxygen and nitrogen species. Angew Chem Int Ed 52:10325–10329
152. Wu C, Hansen SJ, Hou Q, Yu J et al (2011) Design of highly emissive polymer dot bioconjugates for in vivo tumor targeting. Angew Chem Int Ed 50:3430–3434
153. Pu K, Chattopadhyay N, Rao J (2016) Recent advances of semiconducting polymer nanoparticles in in vivo molecular imaging. J Control Release 240:312–322
154. Liu H-Y, Wu P-J, Kuo S-Y, Chen C-P et al (2015) Quinoxaline-based polymer dots with ultrabright red to near-infrared fluorescence for in vivo biological imaging. J Am Chem Soc 137:10420–10429
155. Pu K, Shuhendler AJ, Valta MP, Cui L et al (2014) Phosphorylcholine-coated semiconducting polymer nanoparticles as rapid and efficient labeling agents for in vivo cell tracking. Adv Healthc Mater 3:1292–1298

156. Ding D, Li K, Zhu Z, Pu K-Y et al (2011) Conjugated polyelectrolyte-cisplatin complex nanoparticles for simultaneous in vivo imaging and drug tracking. Nanoscale 3:1997–2002
157. Fu L, Sun C, Yan L (2015) Galactose targeted pH-responsive copolymer conjugated with near infrared fluorescence probe for imaging of intelligent drug delivery. ACS Appl Mater Interfaces 7:2104–2115
158. Koo H, Lee H, Lee S, Min KH et al (2010) In vivo tumor diagnosis and photodynamic therapy via tumoral pH-responsive polymeric micelles. Chem Commun 46:5668–5670
159. Shen S, Wang Q (2013) Rational tuning the optical properties of metal sulfide nanocrystals and their applications. Chem Mater 25:1166–1178
160. Jing L, Kershaw SV, Li Y, Huang X et al (2016) Aqueous based semiconductor nanocrystals. Chem Rev 116:10623–10730
161. Lim SJ, Ma L, Schleife A, Smith AM (2016) Quantum dot surface engineering: toward inert fluorophores with compact size and bright, stable emission. Coord Chem Rev 320–321:216–237
162. He Y, Zhong Y, Su Y, Lu Y et al (2011) Water-dispersed near-infrared-emitting quantum dots of ultrasmall sizes for in vitro and in vivo imaging. Angew Chem Int Ed 50:5695–5698
163. Gu Y-P, Cui R, Zhang Z-L, Xie Z-X et al (2012) Ultrasmall near-infrared Ag_2Se quantum dots with tunable fluorescence for in vivo imaging. J Am Chem Soc 134:79–82
164. Wang J, Lu Y, Peng F, Zhong Y et al (2013) Photostable water-dispersible NIR-emitting CdTe/CdS/ZnS core–shell–shell quantum dots for high-resolution tumor targeting. Biomaterials 34:9509–9518
165. Wang Y, Hu R, Lin G, Law W-C et al (2013) Optimizing the aqueous phase synthesis of CdTe quantum dots using mixed-ligands system and their applications for imaging of live cancer cells and tumors in vivo. RSC Adv 3:8899–8908
166. Chen L-N, Wang J, Li W-T, Han H-Y (2012) Aqueous one-pot synthesis of bright and ultrasmall CdTe/CdS near-infrared-emitting quantum dots and their application for tumor targeting in vivo. Chem Commun 48:4971–4973
167. Kikushima K, Kita S, Higuchi H (2013) A non-invasive imaging for the in vivo tracking of high-speed vesicle transport in mouse neutrophils. Sci Rep 3:1913
168. Chen G, Tian F, Zhang Y, Zhang Y et al (2014) Tracking of transplanted human mesenchymal stem cells in living mice using near-infrared Ag_2S quantum dots. Adv Funct Mater 24:2481–2488
169. Hasegawa M, Tsukasaki Y, Ohyanagi T, Jin T (2013) Bioluminescence resonance energy transfer coupled near-infrared quantum dots using GST-tagged luciferase for in vivo imaging. Chem Commun 49:228–230
170. Yang K, Zhang F-J, Tang H, Zhao C et al (2011) In-vivo imaging of oral squamous cell carcinoma by EGFR monoclonal antibody conjugated near-infrared quantum dots in mice. Int J Nanomedicine 6:1739–1745
171. Yong K-T, Roy I, Law W-C, Hu R (2010) Synthesis of cRGD-peptide conjugated near-infrared CdTe/ZnSe core-shell quantum dots for in vivo cancer targeting and imaging. Chem Commun 46:7136–7138
172. Li C, Ji Y, Wang C, Liang S et al (2014) BRCAA1 antibody- and Her2 antibody-conjugated amphiphilic polymer engineered CdSe/ZnS quantum dots for targeted imaging of gastric cancer. Nanoscale Res Lett 9:244
173. Yuan Y, Zhang J, An L, Cao Q et al (2014) Oligomeric nanoparticles functionalized with NIR-emitting CdTe/CdS QDs and folate for tumor-targeted imaging. Biomaterials 35:7881–7886
174. Liu L, Yong K-T, Roy I, Law W-C et al (2012) Bioconjugated pluronic triblock-copolymer micelle-encapsulated quantum dots for targeted imaging of cancer: in vitro and in vivo studies. Theranostics 2:705–713
175. Liu L-w, Hu S-y, Pan Y, Zhang J-q et al (2014) Optimizing the synthesis of CdS/ZnS core/shell semiconductor nanocrystals for bioimaging applications. Beilstein J Nanotechnol 5:919–926

176. Ding H, Yong K-T, Law W-C, Roy I et al (2011) Non-invasive tumor detection in small animals using novel functional Pluronic nanomicelles conjugated with anti-mesothelin antibody. Nanoscale 3:1813–1822
177. Guo W, Sun X, Jacobson O, Yan X et al (2015) Intrinsically radioactive [^{64}Cu]CuInS/ZnS quantum dots for PET and optical imaging: improved radiochemical stability and controllable cerenkov luminescence. ACS Nano 9:488–495
178. Andrasfalvy BK, Galinanes GL, Huber D, Barbic M et al (2014) Quantum dot-based multiphoton fluorescent pipettes for targeted neuronal electrophysiology. Nat Method 11:1237–1241
179. Xu X, Ray R, Gu Y, Ploehn HJ et al (2004) Electrophoretic analysis and purification of fluorescent single-walled carbon nanotube fragments. J Am Chem Soc 126:12736–12737
180. Yang S-T, Cao L, Luo PG, Lu F et al (2009) Carbon dots for optical imaging in vivo. J Am Chem Soc 131:11308–11309
181. Baker SN, Baker GA (2010) Luminescent carbon nanodots: emergent nanolights. Angew Chem Int Ed 49:6726–6744
182. Liu J-H, Anilkumar P, Cao L, Wang X et al (2010) Cytotoxicity evaluations of fluorescent carbon nanoparticles. Nano Life 01:153–161
183. Luo PG, Sahu S, Yang S-T, Sonkar SK et al (2013) Carbon "quantum" dots for optical bioimaging. J Mater Chem B 1:2116–2127
184. Sharker SM, Kim SM, Lee JE, Jeong JH et al (2015) In situ synthesis of luminescent carbon nanoparticles toward target bioimaging. Nanoscale 7:5468–5475
185. Yuan F, Li S, Fan Z, Meng X et al (2016) Shining carbon dots: synthesis and biomedical and optoelectronic applications. Nano Today 11:565–586
186. Li H, Kang Z, Liu Y, Lee S-T (2012) Carbon nanodots: synthesis, properties and applications. J Mater Chem 22:24230–24253
187. Wang Y, Hu A (2014) Carbon quantum dots: synthesis, properties and applications. J Mater Chem C 2:6921–6939
188. Roy P, Chen P-C, Periasamy AP, Chen Y-N et al (2015) Photoluminescent carbon nanodots: synthesis, physicochemical properties and analytical applications. Mater Today 18:447–458
189. Liu X, Pang J, Xu F, Zhang X (2016) Simple approach to synthesize amino-functionalized carbon dots by carbonization of chitosan. Sci Rep 6:31100
190. Zhang J, Yu S-H (2016) Carbon dots: large-scale synthesis, sensing and bioimaging. Mater Today 19:382–393
191. Nguyen V, Si J, Yan L, Hou X (2015) Electron–hole recombination dynamics in carbon nanodots. Carbon 95:659–663
192. Wang F, Pang S, Wang L, Li Q et al (2010) One-step synthesis of highly luminescent carbon dots in noncoordinating solvents. Chem Mater 22:4528–4530
193. Li X, Wang H, Shimizu Y, Pyatenko A et al (2011) Preparation of carbon quantum dots with tunable photoluminescence by rapid laser passivation in ordinary organic solvents. Chem Commun 47:932–934
194. Li H, He X, Liu Y, Huang H et al (2011) One-step ultrasonic synthesis of water-soluble carbon nanoparticles with excellent photoluminescent properties. Carbon 49:605–609
195. Huang X, Zhang F, Zhu L, Choi KY et al (2013) Effect of injection routes on the biodistribution, clearance, and tumor uptake of carbon dots. ACS Nano 7:5684–5693
196. Huang P, Lin J, Wang X, Wang Z et al (2012) Light-triggered theranostics based on photosensitizer-conjugated carbon dots for simultaneous enhanced-fluorescence imaging and photodynamic therapy. Adv Mater 24:5104–5110
197. Kong B, Zhu A, Ding C, Zhao X et al (2012) Carbon dot-based inorganic–organic nanosystem for two-photon imaging and biosensing of pH variation in living cells and tissues. Adv Mater 24:5844–5848
198. Wang X, Liu Z (2012) Carbon nanotubes in biology and medicine: an overview. Chin Sci Bull 57:167–180

199. O'Connell MJ, Bachilo SM, Huffman CB, Moore VC et al (2002) Band gap fluorescence from individual single-walled carbon nanotubes. Science 297:593–596
200. Welsher K, Liu Z, Sherlock SP, Robinson JT et al (2009) A route to brightly fluorescent carbon nanotubes for near-infrared imaging in mice. Nat Nanotechnol 4:773–780
201. Hong G, Tabakman SM, Welsher K, Wang H et al (2010) Metal-enhanced fluorescence of carbon nanotubes. J Am Chem Soc 132:15920–15923
202. Joselevich E, Dai H, Liu J, Hata K et al (2008) In: Jorio A, Dresselhaus G, Dresselhaus MS (eds) Carbon nanotubes: advanced topics in the synthesis, structure, properties and applications. Springer, Berlin/Heidelberg, pp 101–165
203. Hong H, Gao T, Cai W (2009) Molecular imaging with single-walled carbon nanotubes. Nano Today 4:252–261
204. Liu Z, Tabakman S, Welsher K, Dai H (2009) Carbon nanotubes in biology and medicine: in vitro and in vivo detection, imaging and drug delivery. Nano Res 2:85–120
205. Wu H-C, Chang X, Liu L, Zhao F et al (2010) Chemistry of carbon nanotubes in biomedical applications. J Mater Chem 20:1036–1052
206. Huang H, Zou M, Xu X, Liu F et al (2011) Near-infrared fluorescence spectroscopy of single-walled carbon nanotubes and its applications. TrAC Trends Anal Chem 30:1109–1119
207. Liu Z, Yang K, Lee S-T (2011) Single-walled carbon nanotubes in biomedical imaging. J Mater Chem 21:586–598
208. Gong H, Peng R, Liu Z (2013) Carbon nanotubes for biomedical imaging: the recent advances. Adv Drug Deliv Rev 65:1951–1963
209. Mu B, Zhang J, McNicholas TP, Reuel NF et al (2014) Recent advances in molecular recognition based on nanoengineered platforms. Acc Chem Res 47:979–988
210. Welsher K, Sherlock SP, Dai H (2011) Deep-tissue anatomical imaging of mice using carbon nanotube fluorophores in the second near-infrared window. Proc Natl Acad Sci 108:8943–8948
211. Diao S, Hong G, Robinson JT, Jiao L et al (2012) Chirality enriched (12,1) and (11,3) single-walled carbon nanotubes for biological imaging. J Am Chem Soc 134:16971–16974
212. Robinson JT, Hong G, Liang Y, Zhang B et al (2012) In vivo fluorescence imaging in the second near-infrared window with long circulating carbon nanotubes capable of ultrahigh tumor uptake. J Am Chem Soc 134:10664–10669
213. Yi H, Ghosh D, Ham M-H, Qi J et al (2012) M13 phage-functionalized single-walled carbon nanotubes as nanoprobes for second near-infrared window fluorescence imaging of targeted tumors. Nano Lett 12:1176–1183
214. Shen H, Zhang L, Liu M, Zhang Z (2012) Biomedical applications of graphene. Theranostics 2:283–294
215. Shen J, Zhu Y, Yang X, Li C (2012) Graphene quantum dots: emergent nanolights for bioimaging, sensors, catalysis and photovoltaic devices. Chem Commun 48:3686–3699
216. Gollavelli G, Ling Y-C (2012) Multi-functional graphene as an in vitro and in vivo imaging probe. Biomaterials 33:2532–2545
217. Yang K, Feng L, Shi X, Liu Z (2013) Nano-graphene in biomedicine: theranostic applications. Chem Soc Rev 42:530–547
218. Li L, Wu G, Yang G, Peng J et al (2013) Focusing on luminescent graphene quantum dots: current status and future perspectives. Nanoscale 5:4015–4039
219. Nguyen KT, Zhao Y (2014) Integrated graphene/nanoparticle hybrids for biological and electronic applications. Nanoscale 6:6245–6266
220. Zhang H, Gruner G, Zhao Y (2013) Recent advancements of graphene in biomedicine. J Mater Chem B 1:2542–2567
221. Zhang J, Yang H, Shen G, Cheng P et al (2010) Reduction of graphene oxide vial-ascorbic acid. Chem Commun 46:1112–1114
222. Nurunnabi M, Khatun Z, Reeck GR, Lee DY et al (2013) Near infrared photoluminescent graphene nanoparticles greatly expand their use in noninvasive biomedical imaging. Chem Commun 49:5079–5081

223. Shen J, Zhu Y, Chen C, Yang X et al (2011) Facile preparation and upconversion luminescence of graphene quantum dots. Chem Commun 47:2580–2582
224. Wu X, Tian F, Wang W, Chen J et al (2013) Fabrication of highly fluorescent graphene quantum dots using L-glutamic acid for in vitro/in vivo imaging and sensing. J Mater Chem C 1:4676–4684
225. Abdullah Al N, Lee J-E, In I, Lee H et al (2013) Target delivery and cell imaging using hyaluronic acid-functionalized graphene quantum dots. Mol Pharm 10:3736–3744
226. Liu Q, Guo B, Rao Z, Zhang B et al (2013) Strong two-photon-induced fluorescence from photostable, biocompatible nitrogen-doped graphene quantum dots for cellular and deep-tissue imaging. Nano Lett 13:2436–2441
227. Qian J, Wang D, Cai F-H, Xi W et al (2012) Observation of multiphoton-induced fluorescence from graphene oxide nanoparticles and applications in in vivo functional bioimaging. Angew Chem Int Ed 51:10570–10575
228. Yang K, Hu L, Ma X, Ye S et al (2012) Multimodal imaging guided photothermal therapy using functionalized graphene nanosheets anchored with magnetic nanoparticles. Adv Mater 24:1868–1872
229. Wang Y, Wang H, Liu D, Song S et al (2013) Graphene oxide covalently grafted upconversion nanoparticles for combined NIR mediated imaging and photothermal/photodynamic cancer therapy. Biomaterials 34:7715–7724
230. Mochalin VN, Shenderova O, Ho D, Gogotsi Y (2012) The properties and applications of nanodiamonds. Nat Nanotechnol 7:11–23
231. Danilenko VV (2004) On the history of the discovery of nanodiamond synthesis. Phys Solid State 46:595–599
232. Kuo Y, Hsu T-Y, Wu Y-C, Chang H-C (2013) Fluorescent nanodiamond as a probe for the intercellular transport of proteins in vivo. Biomaterials 34:8352–8360
233. Wu T-J, Tzeng Y-K, Chang W-W, Cheng C-A et al (2013) Tracking the engraftment and regenerative capabilities of transplanted lung stem cells using fluorescent nanodiamonds. Nat Nanotechnol 8:682–689
234. Mohan N, Chen C-S, Hsieh H-H, Wu Y-C et al (2010) In vivo imaging and toxicity assessments of fluorescent nanodiamonds in caenorhabditis elegans. Nano Lett 10:3692–3699
235. Chang B-M, Lin H-H, Su L-J, Lin W-D et al (2013) Highly fluorescent nanodiamonds protein-functionalized for cell labeling and targeting. Adv Funct Mater 23:5737–5745
236. Tzeng Y-K, Faklaris O, Chang B-M, Kuo Y et al (2011) Superresolution imaging of albumin-conjugated fluorescent nanodiamonds in cells by stimulated emission depletion. Angew Chem Int Ed 50:2262–2265
237. Lin H-H, Lee H-W, Lin R-J, Huang C-W et al (2015) Tracking and finding slow-proliferating/quiescent cancer stem cells with fluorescent nanodiamonds. Small 11:4394–4402
238. Alhaddad A, Adam M-P, Botsoa J, Dantelle G et al (2011) Nanodiamond as a vector for siRNA delivery to ewing sarcoma cells. Small 7:3087–3095
239. Havlik J, Petrakova V, Rehor I, Petrak V et al (2013) Boosting nanodiamond fluorescence: towards development of brighter probes. Nanoscale 5:3208–3211
240. Igarashi R, Yoshinari Y, Yokota H, Sugi T et al (2012) Real-time background-free selective imaging of fluorescent nanodiamonds in vivo. Nano Lett 12:5726–5732
241. Chen G, Ohulchanskyy TY, Kumar R, Ågren H et al (2010) Ultrasmall monodisperse $NaYF_4$:Yb^{3+}/Tm^{3+} nanocrystals with enhanced near-infrared to near-infrared upconversion photoluminescence. ACS Nano 4:3163–3168
242. Wang Y, Cai R, Liu Z (2011) Controlled synthesis of $NaYF_4$:Yb,Er nanocrystals with upconversion fluorescence via a facile hydrothermal procedure in aqueous solution. CrystEngComm 13:1772–1774
243. Ye X, Collins JE, Kang Y, Chen J et al (2010) Morphologically controlled synthesis of colloidal upconversion nanophosphors and their shape-directed self-assembly. Proc Natl Acad Sci 107:22430–22435

244. Yang D, Li C, Li G, Shang M et al (2011) Colloidal synthesis and remarkable enhancement of the upconversion luminescence of $BaGdF_5:Yb^{3+}/Er^{3+}$ nanoparticles by active-shell modification. J Mater Chem 21:5923–5927
245. Budijono SJ, Shan J, Yao N, Miura Y et al (2010) Synthesis of stable block-copolymer-protected $NaYF_4:Yb^{3+},Er^{3+}$ up-converting phosphor nanoparticles. Chem Mater 22:311–318
246. Pedroni M, Piccinelli F, Passuello T, Giarola M et al (2011) Lanthanide doped upconverting colloidal CaF2 nanoparticles prepared by a single-step hydrothermal method: toward efficient materials with near infrared-to-near infrared upconversion emission. Nanoscale 3:1456–1460
247. Liu Q, Li C, Yang T, Yi T et al (2010) "Drawing" upconversion nanophosphors into water through host-guest interaction. Chem Commun 46:5551–5553
248. Liu Q, Chen M, Sun Y, Chen G et al (2011) Multifunctional rare-earth self-assembled nanosystem for tri-modal upconversion luminescence/fluorescence/positron emission tomography imaging. Biomaterials 32:8243–8253
249. Shan J, Kong W, Wei R, Yao N et al (2010) An investigation of the thermal sensitivity and stability of the β-$NaYF_4$:Yb,Er upconversion nanophosphors. J Appl Phys 107:054901
250. Wang F, Wang J, Liu X (2010) Direct evidence of a surface quenching effect on size-dependent luminescence of upconversion nanoparticles. Angew Chem Int Ed 49:7456–7460
251. Hu D, Chen M, Gao Y, Li F et al (2011) A facile method to synthesize superparamagnetic and up-conversion luminescent $NaYF_4$:Yb,Er/Tm@SiO_2@Fe_3O_4 nanocomposite particles and their bioapplication. J Mater Chem 21:11276–11282
252. Zhou J, Yao L, Li C, Li F (2010) A versatile fabrication of upconversion nanophosphors with functional-surface tunable ligands. J Mater Chem 20:8078–8085
253. Wang Z-L, Hao J, Chan HLW, Law G-L et al (2011) Simultaneous synthesis and functionalization of water-soluble up-conversion nanoparticles for in-vitro cell and nude mouse imaging. Nanoscale 3:2175–2181
254. Cao T, Yang Y, Gao Y, Zhou J et al (2011) High-quality water-soluble and surface-functionalized upconversion nanocrystals as luminescent probes for bioimaging. Biomaterials 32:2959–2968
255. Chen C, Sun L-D, Li Z-X, Li L-L et al (2010) Ionic liquid-based route to spherical $NaYF_4$ nanoclusters with the assistance of microwave radiation and their multicolor upconversion luminescence. Langmuir 26:8797–8803
256. Xiong L, Yang T, Yang Y, Xu C et al (2010) Long-term in vivo biodistribution imaging and toxicity of polyacrylic acid-coated upconversion nanophosphors. Biomaterials 31:7078–7085
257. Chen G, Shen J, Ohulchanskyy TY, Patel NJ et al (2012) (α-$NaYbF_4:Tm^{3+}$)/CaF_2 core/shell nanoparticles with efficient near-infrared to near-infrared upconversion for high-contrast deep tissue bioimaging. ACS Nano 6:8280–8287
258. Wang Y-F, Liu G-Y, Sun L-D, Xiao J-W et al (2013) Nd^{3+}-sensitized upconversion nanophosphors: efficient in vivo bioimaging probes with minimized heating effect. ACS Nano 7:7200–7206
259. Zhan Q, Qian J, Liang H, Somesfalean G et al (2011) Using 915 nm laser excited $Tm^{3+}/Er^{3+}/Ho^{3+}$-doped $NaYbF_4$ upconversion nanoparticles for in vitro and deeper in vivo bioimaging without overheating irradiation. ACS Nano 5:3744–3757
260. Sun L-D, Wang Y-F, Yan C-H (2014) Paradigms and challenges for bioapplication of rare earth upconversion luminescent nanoparticles: small size and tunable emission/excitation spectra. Acc Chem Res 47:1001–1009
261. Cheng L, Yang K, Shao M, Lee S-T et al (2011) Multicolor in vivo imaging of upconversion nanoparticles with emissions tuned by luminescence resonance energy transfer. J Phys Chem C 115:2686–2692
262. Liu Y, Chen M, Cao T, Sun Y et al (2013) A cyanine-modified nanosystem for in vivo upconversion luminescence bioimaging of methylmercury. J Am Chem Soc 135:9869–9876
263. Yu X-F, Sun Z, Li M, Xiang Y et al (2010) Neurotoxin-conjugated upconversion nanoprobes for direct visualization of tumors under near-infrared irradiation. Biomaterials 31:8724–8731

264. Liu Q, Sun Y, Yang T, Feng W et al (2011) Sub-10 nm hexagonal lanthanide-doped $NaLuF_4$ upconversion nanocrystals for sensitive bioimaging in vivo. J Am Chem Soc 133:17122–17125
265. Ai X, Lyu L, Zhang Y, Tang Y et al (2017) Remote regulation of membrane channel activity by site-specific localization of lanthanide-doped upconversion nanocrystals. Angew Chem Int Ed 56:3031–3035
266. N. G. Khlebtsov and L. A. Dykman, Optical properties and biomedical applications of plasmonic nanoparticles, J Quant Spectrosc Radiat Transf, 2010, 111: 1–35
267. Shang L, Dong S, Nienhaus GU (2011) Ultra-small fluorescent metal nanoclusters: synthesis and biological applications. Nano Today 6:401–418
268. Liu C-L, Wu H-T, Hsiao Y-H, Lai C-W et al (2011) Insulin-directed synthesis of fluorescent gold nanoclusters: preservation of insulin bioactivity and versatility in cell imaging. Angew Chem Int Ed 50:7056–7060
269. Polavarapu L, Manna M, Xu Q-H (2011) Biocompatible glutathione capped gold clusters as one- and two-photon excitation fluorescence contrast agents for live cells imaging. Nanoscale 3:429–434
270. Shang L, Dorlich RM, Brandholt S, Schneider R et al (2011) Facile preparation of water-soluble fluorescent gold nanoclusters for cellular imaging applications. Nanoscale 3:2009–2014
271. Gao S, Chen D, Li Q, Ye J et al (2014) Near-infrared fluorescence imaging of cancer cells and tumors through specific biosynthesis of silver nanoclusters. Sci Rep 4:4384
272. Nie LB, Xiao XY, Yang HC (2016) Preparation and biomedical applications of gold nanocluster, Jounal of Nanoscience. Nanotechnology 16:8164–8175
273. Kim Y-H, Jeon J, Hong SH, Rhim W-K et al (2011) Tumor targeting and imaging using cyclic RGD-PEGylated gold nanoparticle probes with directly conjugated iodine-125. Small 7:2052–2060
274. Mathew A, Pradeep T (2014) Noble metal clusters: applications in energy, environment, and biology. Part Part Syst Charact 31:1017–1053
275. Qiu L, Chen T, Öçsoy I, Yasun E et al (2015) A cell-targeted, size-photocontrollable, nuclear-uptake nanodrug delivery system for drug-resistant cancer therapy. Nano Lett 15:457–463
276. Wu X, He X, Wang K, Xie C et al (2010) Ultrasmall near-infrared gold nanoclusters for tumor fluorescence imaging in vivo. Nanoscale 2:2244–2249
277. Guo C, Irudayaraj J (2011) Fluorescent Ag clusters via a protein-directed approach as a Hg (II) ion sensor. Anal Chem 83:2883–2889
278. Habeeb Muhammed MA, Verma PK, Pal SK, Retnakumari A et al (2010) Luminescent quantum clusters of gold in bulk by albumin-induced core etching of nanoparticles: metal ion sensing, metal-enhanced luminescence, and biolabeling. Chem Eur J 16:10103–10112
279. Wen F, Dong Y, Feng L, Wang S et al (2011) Horseradish peroxidase functionalized fluorescent gold nanoclusters for hydrogen peroxide sensing. Anal Chem 83:1193–1196
280. Pitchiaya S, Krishnan Y (2006) First blueprint, now bricks: DNA as construction material on the nanoscale. Chem Soc Rev 35:1111–1121
281. Zhou C, Long M, Qin Y, Sun X et al (2011) Luminescent gold nanoparticles with efficient renal clearance. Angew Chem Int Ed 50:3168–3172
282. Sun M, Xu L, Ma W, Wu X et al (2016) Hierarchical plasmonic nanorods and upconversion core–satellite nanoassemblies for multimodal imaging-guided combination phototherapy. Adv Mater 28:898–904
283. Lim WQ, Phua SZ, Xu HV, Sreejith S et al (2016) Recent advances in multifunctional silica-based hybrid nanocarriers for bioimaging and cancer therapy. Nanoscale 8:12510–12519
284. Cheng S-H, Li F-C, Souris JS, Yang C-S et al (2012) Visualizing dynamics of sub-hepatic distribution of nanoparticles using intravital multiphoton fluorescence microscopy. ACS Nano 6:4122–4131
285. Gu L, Hall DJ, Qin Z, Anglin E et al (2013) In vivo time-gated fluorescence imaging with biodegradable luminescent porous silicon nanoparticles. Nat Commun 4:2326

286. Croissant JG, Qi C, Mongin O, Hugues V et al (2015) Disulfide-gated mesoporous silica nanoparticles designed for two-photon-triggered drug release and imaging. J Mater Chem B 3:6456–6461
287. Geng J, Goh CC, Qin W, Liu R et al (2015) Silica shelled and block copolymer encapsulated red-emissive AIE nanoparticles with 50% quantum yield for two-photon excited vascular imaging. Chem Commun 51:13416–13419
288. Wu Y, Shi M, Zhao L, Feng W et al (2014) Visible-light-excited and europium-emissive nanoparticles for highly-luminescent bioimaging in vivo. Biomaterials 35:5830–5839
289. Sreejith S, Ma X, Zhao Y (2012) Graphene oxide wrapping on squaraine-loaded mesoporous silica nanoparticles for bioimaging. J Am Chem Soc 134:17346–17349
290. Nguyen KT, Sreejith S, Joseph J, He T et al (2014) Poly(acrylic acid)-capped and dye-loaded graphene oxide-mesoporous silica: a nano-sandwich for two-photon and photoacoustic dual-mode imaging. Part Part Syst Charact 31:1060–1066
291. Helle M, Rampazzo E, Monchanin M, Marchal F et al (2013) Surface chemistry architecture of silica nanoparticles determine the efficiency of in vivo fluorescence lymph node mapping. ACS Nano 7:8645–8657
292. Xiao Q, Zheng X, Bu W, Ge W et al (2013) A core/satellite multifunctional nanotheranostic for in vivo imaging and tumor eradication by radiation/photothermal synergistic therapy. J Am Chem Soc 135:13041–13048
293. Kumar R, Roy I, Ohulchanskky TY, Vathy LA et al (2010) In vivo biodistribution and clearance studies using multimodal organically modified silica nanoparticles. ACS Nano 4:699–708
294. Wu X, Chang S, Sun X, Guo Z et al (2013) Constructing NIR silica-cyanine hybrid nanocomposite for bioimaging in vivo: a breakthrough in photo-stability and bright fluorescence with large stokes shift. Chem Sci 4:1221–1228
295. Wang R, Zhou L, Wang W, Li X et al (2017) In vivo gastrointestinal drug-release monitoring through second near-infrared window fluorescent bioimaging with orally delivered microcarriers. Nat Commun 8:14702
296. Huang P, Lin J, Wang S, Zhou Z et al (2013) Photosensitizer-conjugated silica-coated gold nanoclusters for fluorescence imaging-guided photodynamic therapy. Biomaterials 34:4643–4654
297. McVey BFP, Tilley RD (2014) Solution synthesis, optical properties, and bioimaging applications of silicon nanocrystals. Acc Chem Res 47:3045–3051
298. Erogbogbo F, Yong K-T, Roy I, Hu R et al (2011) In vivo targeted cancer imaging, sentinel lymph node mapping and multi-channel imaging with biocompatible silicon nanocrystals. ACS Nano 5:413–423